Dual-Regression Retrieval Algorithm for Real-Time Processing of Satellite Ultraspectral Radiances

WILLIAM L. SMITH SR.

Cooperative Institute for Meteorological Satellite Studies, University of Wisconsin—Madison, Madison, Wisconsin, and Hampton University, Hampton, Virginia

ELISABETH WEISZ

Cooperative Institute for Meteorological Satellite Studies, University of Wisconsin—Madison, Madison, Wisconsin

STANISLAV V. KIREEV

Hampton University, Hampton, Virginia

DANIEL K. ZHOU

NASA Langley Research Center, Hampton, Virginia

ZHENGLONG LI AND EVA E. BORBAS

Cooperative Institute for Meteorological Satellite Studies, University of Wisconsin—Madison, Madison, Wisconsin

(Manuscript received 22 August 2011, in final form 23 January 2012)

ABSTRACT

A fast physically based dual-regression (DR) method is developed to produce, in real time, accurate profile and surface- and cloud-property retrievals from satellite ultraspectral radiances observed for both clear- and cloudy-sky conditions. The DR relies on using empirical orthogonal function (EOF) regression ''clear trained'' and ''cloud trained'' retrievals of surface skin temperature, surface-emissivity EOF coefficients, carbon dioxide concentration, cloud-top altitude, effective cloud optical depth, and atmospheric temperature, moisture, and ozone profiles above the cloud and below thin or broken cloud. The cloud-trained retrieval is obtained using cloud-height-classified statistical datasets. The result is a retrieval with an accuracy that is much higher than that associated with the retrieval produced by the unclassified regression method currently used in the International Moderate Resolution Imaging Spectroradiometer/Atmospheric Infrared Sounder (MODIS/AIRS) Processing Package (IMAPP) retrieval system. The improvement results from the fact that the nonlinear dependence of spectral radiance on the atmospheric variables, which is due to cloud altitude and associated atmospheric moisture concentration variations, is minimized as a result of the cloud-height-classification process. The detailed method and results from example applications of the DR retrieval algorithm are presented. The new DR method will be used to retrieve atmospheric profiles from *Aqua* AIRS, MetOp Infrared Atmospheric Sounding Interferometer, and the forthcoming Joint Polar Satellite System ultraspectral radiance data.

1. Introduction

The advent of accurate high-spectral-resolution radiance measurements from satellites has ushered in a new era of global atmospheric sounding applications (Smith 1991; Hilton et al. 2012). Important for weather applications, these new satellite ultraspectral radiance observations permit the retrieval of atmospheric temperature and water vapor profiles with much higher vertical resolution than was achievable with predecessor multispectral lower-spectral-resolution radiance measurements (Smith et al. 2009). The term ultraspectral is used to convey the spectral resolution (i.e., the

Corresponding author address: William L. Smith, Cooperative Institute for Meteorological Satellite Studies, University of Wisconsin—Madison, 1225 West Dayton St., Madison, WI 53706.
E-mail: bill.l.smith@cox.net

DOI: 10.1175/JAMC-D-11-0173.1

wavenumber increment that is resolved divided by the wavenumber of the observation) being better than 1% and providing more than 1000 spectral channels of radiance information. Because the ultraspectral radiance measurements are obtained for thousands of spectral channels, computationally fast methods for retrieving the atmospheric profiles from radiometric data are required for operational use of the data. It is important to use the data from as many spectral channels as possible so as to retrieve atmospheric thermodynamic features with high spatial resolution, because the profile information content and the radiometric signal to noise influencing the retrieval resolution increase with the number of spectral channels utilized in the retrieval process. This improvement is true even when using spectral channels within the radiance spectrum that possess physically redundant information, because the signal to noise affecting the retrieval process increases with the square root of the number of spectral channels used (Smith et al. 2009). Thus, to optimize the real-time use of these ultraspectral radiance data for the weather analysis/forecast operation, computationally efficient linear processing algorithms are required. Furthermore, the earth's surface characteristics and the influence of clouds must be taken into account to maximize the yield of these high-spatial-resolution sounding retrievals over land and under all-sky conditions. Also, because the spectral radiance measurements are nonlinearly dependent on cloud altitude and moisture concentration, classification methods must be used to be able to achieve accurate profiles under all cloud and associated relative humidity conditions. This paper presents a geophysical product retrieval algorithm that meets the requirements mentioned above for the real-time production of accurate atmospheric profile, surface, and cloud products from the satellite ultraspectral-resolution radiance measurements. The retrieval algorithm described below is to be integrated into the Cooperative Institute of Meteorological Satellite Studies (CIMSS) International Moderate Resolution Imaging Spectroradiometer/Atmospheric Infrared Sounder (MODIS/AIRS) Processing Package (IMAPP). It will also form the basis for a new Joint Polar Satellite System Processing Package (JPSSPP), which can be used to process MetOp Infrared Atmospheric Sounding Interferometer (IASI) and National Polar-Orbiting Operational Environmental Satellite System (NPOESS) Preparatory Project (NPP)/Joint Polar Satellite System (JPSS) Cross-Track Infrared Sounder (CrIS) data.

In this paper, section 2 describes the algorithm, including its physical/theoretical basis, the statistical training datasets, radiative transfer model, and quality-control method. Section 3 presents a comparison of the accuracy of the results obtained with this new dual-regression cloud-classified regression algorithm with that associated with the original single-regression unclassified IMAPP algorithm for both statistically independent and statistically dependent validation datasets. The practical significance of the algorithm is shown by the results of two case studies involving its application to AIRS and IASI radiance observations for two intense weather situations: 1) Hurricane Isabel and 2) the Joplin, Missouri, tornado. The paper concludes by summarizing the results and discussing its future applications to the ultraspectral radiance data to be obtained by the JPSS.

2. Method

a. Overview

The development of computationally efficient retrieval methods for application to the large number of spectral radiances provided by an ultraspectral infrared (IR) instrument has been of interest ever since the High-Resolution Interferometer Sounder (HIS) flew on the National Aeronautics and Space Administration (NASA) ER-2 aircraft during the mid-1980s (Smith 1991; Zhou et al. 2005; Blackwell 2005; Liu et al. 2009). The sounding-retrieval method is a fast physical–statistical algorithm intended for the retrieval of atmospheric profiles as well as surface and cloud parameters from satellite ultraspectral radiance observations. The term statistical is used to denote the fact that the solution depends upon the statistical properties of the spectral radiances, atmospheric profiles, surface parameters, and cloud parameters contained in a statistical training dataset. The term physical is used because the solution depends on theoretical calculations of radiance corresponding to the atmospheric, surface, and cloud conditions provided in nine (i.e., one clear and eight different overlapping cloud-height ranges) geophysical-variable statistical training datasets (Zhou et al. 2005). The physical dual-regression (DR) method utilizes two types of eigenvector [empirical orthogonal function (EOF)] regression, ''clear trained'' and ''cloud trained,'' retrievals of surface skin temperature, surface emissivity EOF coefficients (EOFCs), carbon dioxide (CO_2) concentration, cloud-top altitude, effective cloud optical depth, and atmospheric temperature, moisture, and ozone profiles above the cloud and below thin or broken cloud. The clear-trained regression relates the surface and atmospheric-profile parameters to their associated radiance spectra produced by radiative transfer computations assuming clear-sky atmospheric conditions. The cloud-trained regression relates the surface, cloud,

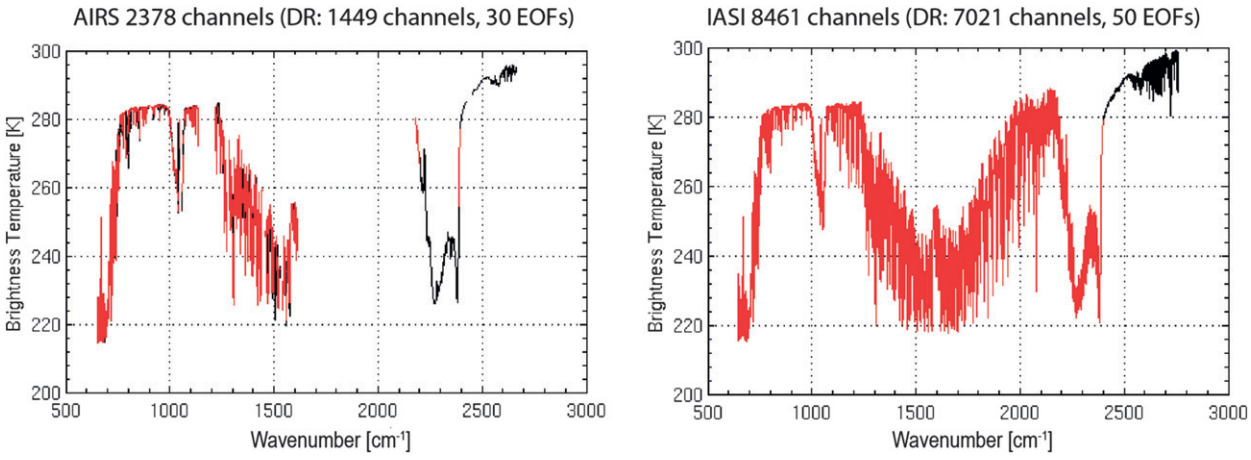

FIG. 1. Global mean (left) AIRS and (right) IASI brightness temperature spectra (black), with the spectral region used for the DR retrieval shown in red.

and atmospheric-profile parameters to their associated radiance spectra calculated using a cloud radiative transfer model, assuming cloud parameters diagnosed from the atmospheric humidity profiles. The initial cloud height and the retrieval cloud-height class for an individual retrieval are specified as a weighted average of the cloud heights produced from the eigenvector regression solutions for the two cloud-height classes that yield values closest to their cloud-class median value. The final value of the "thermal-cloud-top" altitude is assumed to be the altitude below which the clear-trained temperature retrieval remains colder than the cloud-trained temperature profile or a model-analysis temperature profile, whichever is warmer than the clear-trained temperature-profile retrieval. The model analysis temperature profile is obtained from the National Centers for Environmental Prediction (NCEP) Global Data Assimilation System (GDAS). The DR method combines the clear-trained retrieval with the cloud-trained retrieval to produce accurate retrievals for both clear- and cloudy-sky conditions. The final profile retrieval is taken as the clear-trained solution above the thermal-cloud-top level and as the cloud-trained solution below the thermal-cloud-top level. Note that the profile below the thermal-cloud-top level is rejected (i.e., declared to be missing) when the maximum difference between the cloud-trained and clear-trained solutions exceeds 25 K. The "highest possible" cloud top is considered to be the higher of the thermal cloud top and the highest altitude above 300 hPa in which the clear-trained retrieved relative humidity exceeds 70%. The theoretical calculations of radiance required to produce the nine sets of regression coefficients used for the retrieval are performed only once, offline, for global sets of the geophysical data so that the retrieval process is very fast. The cloud-altitude-stratified DR retrieval procedure alleviates the need for a more-time-consuming optimal-estimation matrix-inversion physical retrieval to account for the nonlinear dependence of spectral radiance on cloud altitude and atmospheric moisture.

b. *Physical/mathematical basis*

The physical–statistical-regression sounding-retrieval algorithm has the form

$$\mathbf{q}_{\text{ret}} = \mathbf{q}_0 + (\mathbf{r}_m - \mathbf{r}_0)\mathbf{C}, \tag{1}$$

where the vector $\mathbf{r}_m$ is the measured radiance spectrum and the retrieval vector $\mathbf{q}_{\text{ret}}$ represents the retrieved atmospheric profiles of temperature, water vapor, ozone, CO_2 column concentration, surface skin temperature, surface-emissivity EOFCs, cloud-top pressure, and cloud optical depth. Here, $\mathbf{C}$ is a statistical-regression

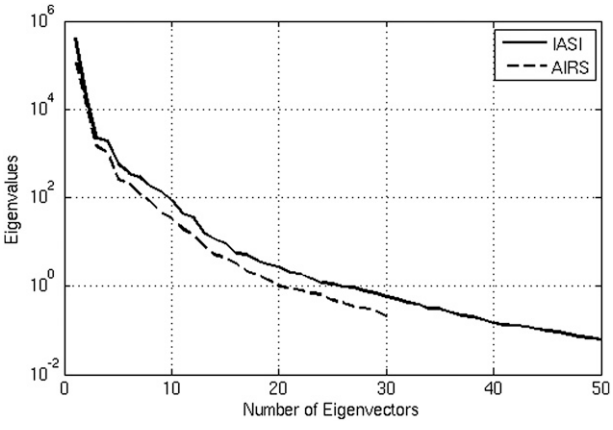

FIG. 2. Comparison of eigenvalues of the AIRS (dashed line) and IASI (solid line) radiance spectra corresponding to the statistical samples of soundings used to derive the DR retrieval coefficients.

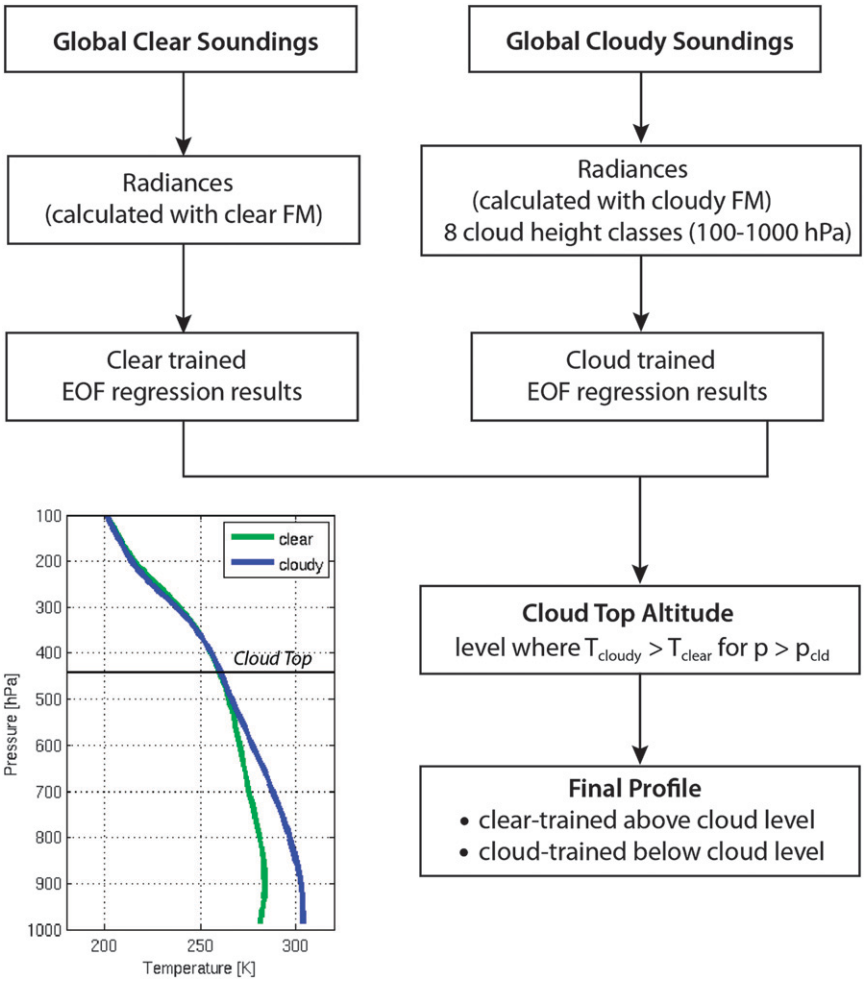

FIG. 3. Schematic diagram of the DR retrieval process; FM refers to the "forward model" used for radiative transfer calculations.

coefficient matrix computed from surface and atmospheric state vector and associated computed radiance spectra deviations from ensemble means $\mathbf{q}_o$ and $\mathbf{r}_o$, respectively. The statistical-regression coefficient matrix $\mathbf{C}$ is given by

$$\mathbf{C} = (\mathbf{R}'^{\mathrm{T}}\mathbf{R}' + \mathbf{E}^{\mathrm{T}}\mathbf{E})^{-1}\mathbf{R}'^{\mathrm{T}}\mathbf{Q}', \qquad (2)$$

where the matrices $\mathbf{Q}$ and $\mathbf{R}$ are climatological ensembles of atmospheric states (i.e., surface and cloud parameters, CO_2 column concentration, and atmospheric temperature, water vapor, and ozone profiles), and associated computed radiance spectra. The prime symbol represents a deviation from the initial conditions $\mathbf{q}_o$ and $\mathbf{r}_o$. Here, $\mathbf{E}^{\mathrm{T}}\mathbf{E}$ is a statistical covariance of spectral radiance noise. To insure stability in the solution for $\mathbf{C}$, the radiances used in (2) are expressed in terms of a limited number of eigenvectors of the training-dataset-calculated radiance covariance matrix [i.e., eigenvector regression (Smith and Woolf 1976; Smith et al. 2004, 2005; Zhou et al. 2005) is used]. Thus, the radiance errors $\mathbf{E}^{\mathrm{T}}\mathbf{E}$ are expressed in terms of the errors in the EOFCs resulting from expected measurement and forward-model error. For AIRS, 1449 of the 2378 available spectral channel radiances, expressed in terms of 30 EOFCs (Weisz et al. 2007a), are used; for IASI, 7021 of the 8461 available spectral channel radiances, expressed in terms of 50 EOFCs, are used. Figure 1 shows the spectral coverage of the channels used for the DR AIRS and IASI retrievals. Descriptions of the AIRS and IASI can be found, respectively, in Chahine et al. (2006) and Hilton et al. (2012). Figure 2 shows the comparison of eigenvalues of the AIRS and IASI radiance spectra derived from the statistical samples of clear and cloudy soundings used to derive the DR retrieval coefficients. It can be seen from Fig. 2 that the higher-spectral-resolution IASI radiance spectra provide more linearly independent pieces of information than do the AIRS

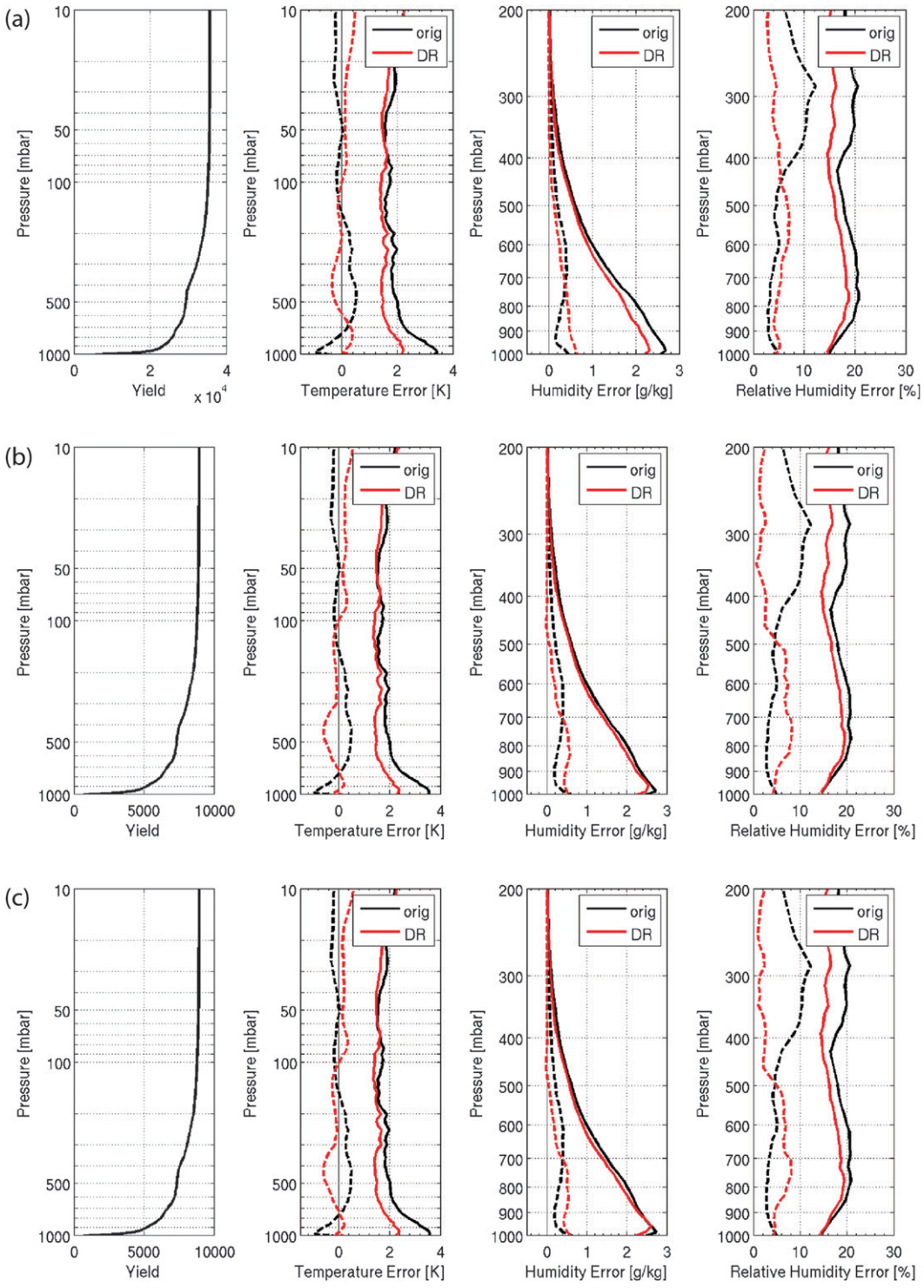

FIG. 4. Comparison of bias (dashed curves) and std dev (solid curves) errors of the original IMAPP unstratified retrievals (black) and the cloud-height-stratified DR retrievals (red) from radiances simulated for the training dataset for (a) the entire sample of soundings using regression coefficients derived from the entire dependent sample of soundings, (b) 25% of the statistical sample using regression coefficients that are based on the independent remaining 75% of the statistical sample of soundings (i.e., independent sample statistics), and (c) the same 25% of the statistical sample used for (b), but on the basis of regression coefficients derived from the entire dependent statistical sample of soundings (i.e., dependent sample statistics).

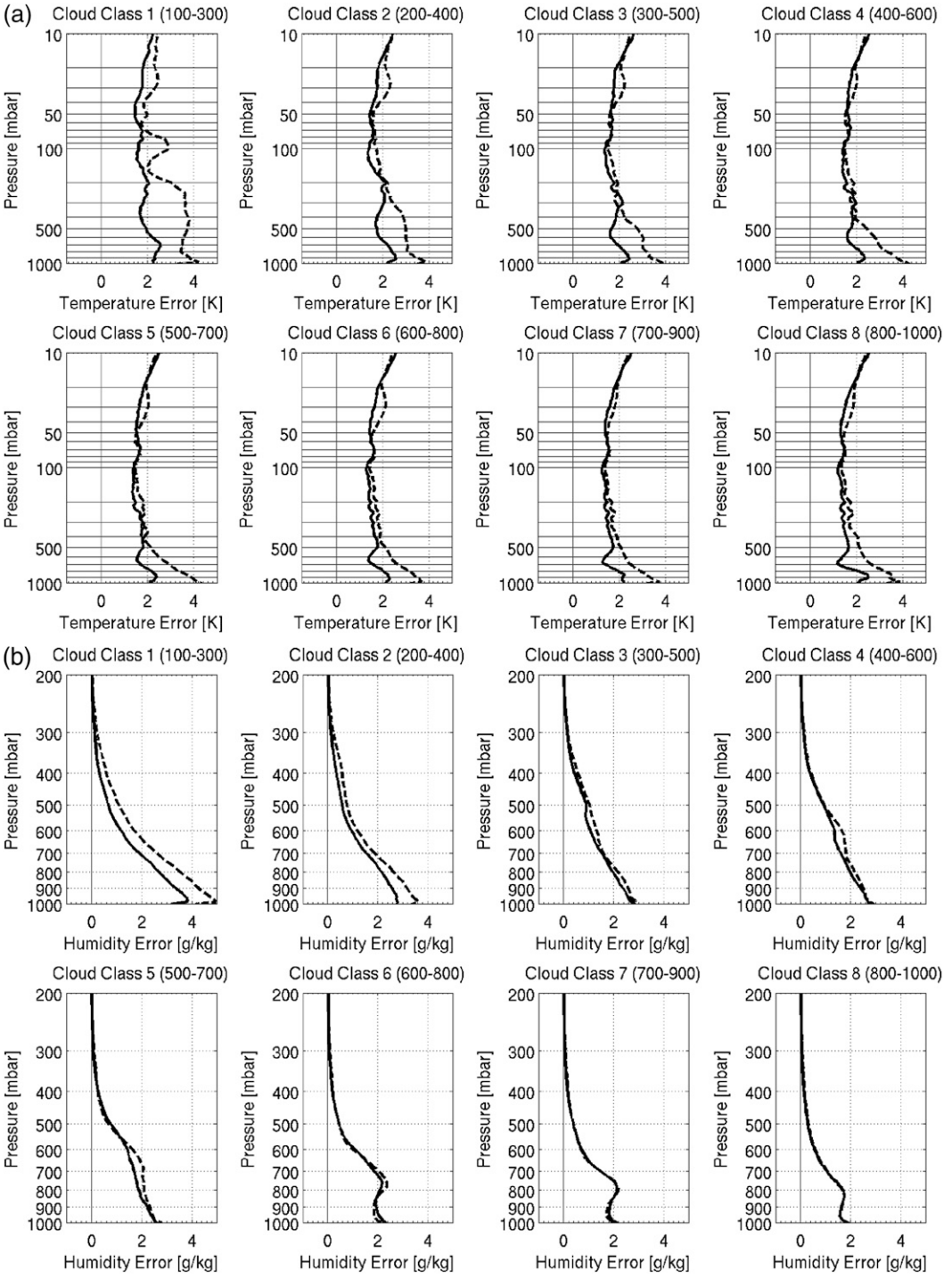

FIG. 5. (a) Comparison of AIRS training-dataset RMS deviation errors for the original IMAPP unstratified retrievals (dashed curves) and the cloud-height-stratified DR retrievals (solid curves) from radiances simulated for the training dataset for different cloud-height classes for (a) temperature, (b) humidity, and (c) relative humidity.

spectra. Thus, more EOFCs can be used as regression predictors for IASI retrievals than for AIRS retrievals.

The DR relies on using eigenvector-regression clear-trained and cloud-trained retrievals of surface skin temperature, surface emissivity principal-component scores, CO_2 concentration, cloud-top altitude, effective cloud optical depth, and atmospheric temperature, moisture, and ozone profiles above the cloud and below thin

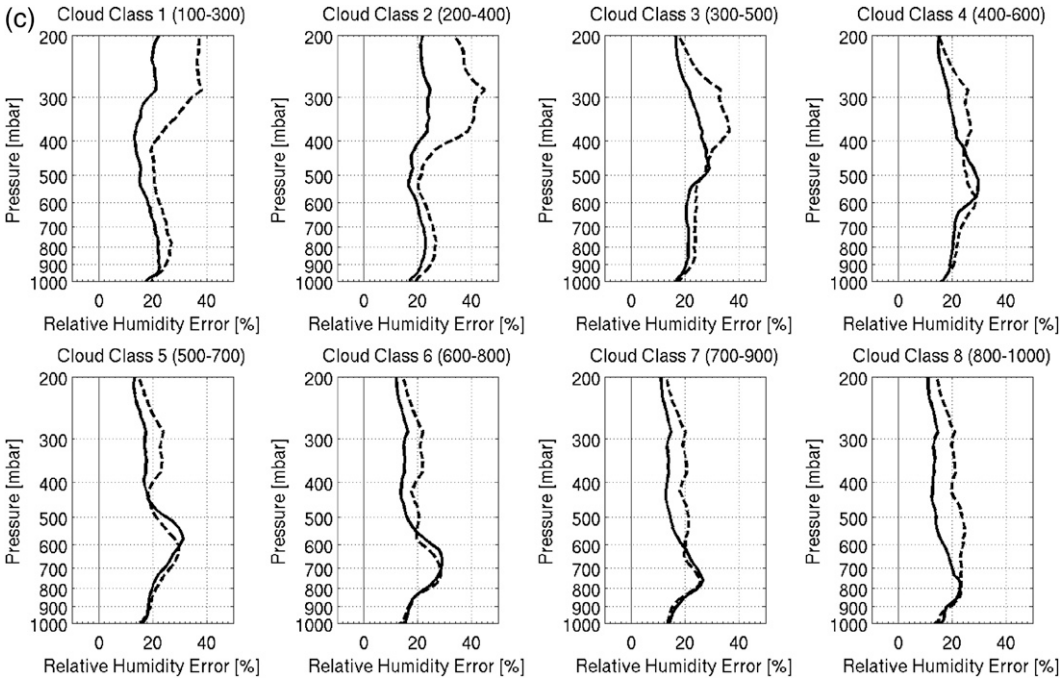

FIG. 5. (*Continued*)

or scattered cloud. The clear-trained regression is a relation between the retrieval variables and the associated clear-sky radiance spectra. The cloud-trained regression is a relation between the retrieval variables and the associated cloudy-sky radiance spectra. Thus, applying the clear-trained regression solution to cloud-attenuated radiances will produce a temperature profile that is colder below the cloud level than the true profile by a degree dependent upon the altitude, temperature, and optical depth of the cloud. In the ideal case, if the cloud is opaque, the clear-trained temperature profile retrieval should be correct above the cloud level and isothermal below the cloud level with a temperature value equal to the cloud-top temperature. On the other hand, the cloud-trained regression retrieval from cloud-attenuated radiances should produce a profile below the cloud that is much closer to the true profile, the accuracy being dependent on the height and optical thickness of the cloud. In the case of an overcast opaque cloud, the cloud-trained retrieval below the cloud is a pure statistical extrapolation of the profile retrieved above the cloud top, since there is no radiance information from below the cloud to influence the retrieval. Under cloudless-sky conditions, the clear-trained and the cloud-trained retrievals should be nearly identical. Thus, the difference between clear-trained and cloud-trained retrievals below the cloud is a measure of the expected cloud-induced error in the cloud-trained retrieval below the cloud. In the clear-sky case, and for the clear sky above the cloud top, the clear-trained retrieval is expected to be slightly more accurate than the cloud-trained retrieval because of the much smaller variance of clear-sky radiances as compared with the cloudy-sky radiances, affecting the regression-retrieval coefficients, that is, matrix $\mathbf{C}$ as defined in (2). Figure 3 shows a schematic of the DR retrieval process.

c. Statistical training datasets

The clear-trained regression relations are derived using a training database consisting of 15 704 profiles of temperature, moisture, and ozone at 101 pressure levels for clear-sky conditions, as defined from the temperature and humidity profiles (Borbas et al. 2005). The profiles, distributed uniformly in both space and time, are taken from the National Oceanic and Atmospheric Administration (NOAA)-88 radiosonde dataset, a European Centre for Medium-Range Weather Forecasts training set, the Thermodynamic Initial Guess Retrieval (TIGR)-3 radiosonde dataset, and radiosondes from the Sahara desert. Ozonesondes were taken from eight NOAA Climate Monitoring and Diagnostics Laboratory sites; quality checks were applied to all of the profiles along with the following saturation criterion: for clear-sky conditions, the relative humidity value of the profiles must be less than 99% at each level above 250-hPa pressure altitude level. In addition, it was required that the original sounding top of pressure be less than 30 hPa for radiosondes and 10 hPa for

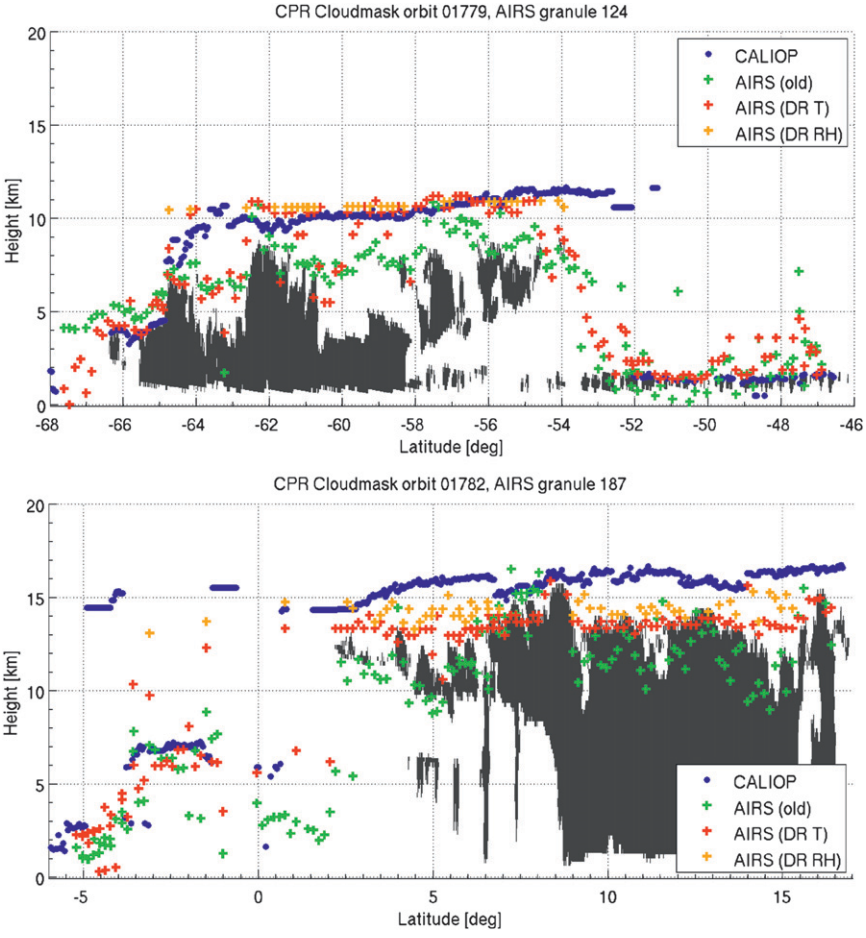

FIG. 6. Comparison of DR cloud heights (red and orange plus signs) and those obtained by the old IMAPP algorithm (green plus signs) with those observed by the CALIOP lidar (blue dots) for AIRS granules (top) 124 and (bottom) 187 for 28 Aug 2006. The background (black shading) shows *CloudSat's* L2 CPR Cloud Mask product.

ozonesondes. A technique to extend the temperature, moisture, and ozone profiles into the upper atmosphere, above the level of existing data, that produces results that are physically consistent with atmospheric measurements from below was implemented. Where ozone data were not included with the original profiles, a time- and location-independent temperature-profile predictor regression-based algorithm was used for specifying the ozone profiles. The regressions are expressed in terms of level values, as opposed to layer averages, for the 101 fixed pressures. The surface pressure supplied by the NCEP Global Forecast System (GFS) or by GDAS (if GFS is not available) is used to determine the lowest valid level of each retrieval.

The cloudy-sky training dataset consists of a total of 19 948 profiles, of which 11 979 profiles are cloudy profiles and the remaining 7969 come from the clear set, with cloud parameters assigned to all of the profiles as described below. The relative humidity and temperature were used to determine whether the profile was cloudy or clear and to assign cloud-top pressure using a technique described by Minnis et al. (2005). Here, a relative humidity threshold profile (Jin et al. 2006), in which the threshold changed smoothly with altitude in the range between 55% and 95%, was used to produce a relatively uniform distribution of cloud-top altitude for the statistical ensemble of soundings that form the cloudy-sky training dataset. For each cloud, a cloud optical thickness ranging between 0.01 and 10 and an effective cloud-particle diameter between 10 and 50 μm for ice crystals and between 5 and 35 μm for water droplets were assigned using a uniform-distribution random-number generator. Ice clouds were assumed to be between 600 hPa and the tropopause, whereas water clouds were assumed to be between 400 hPa and the surface, depending on the temperature of the cloud. The cloudy soundings were then assigned to eight different overlapping cloud-height classes: 100–300, 200–400, 300–500,

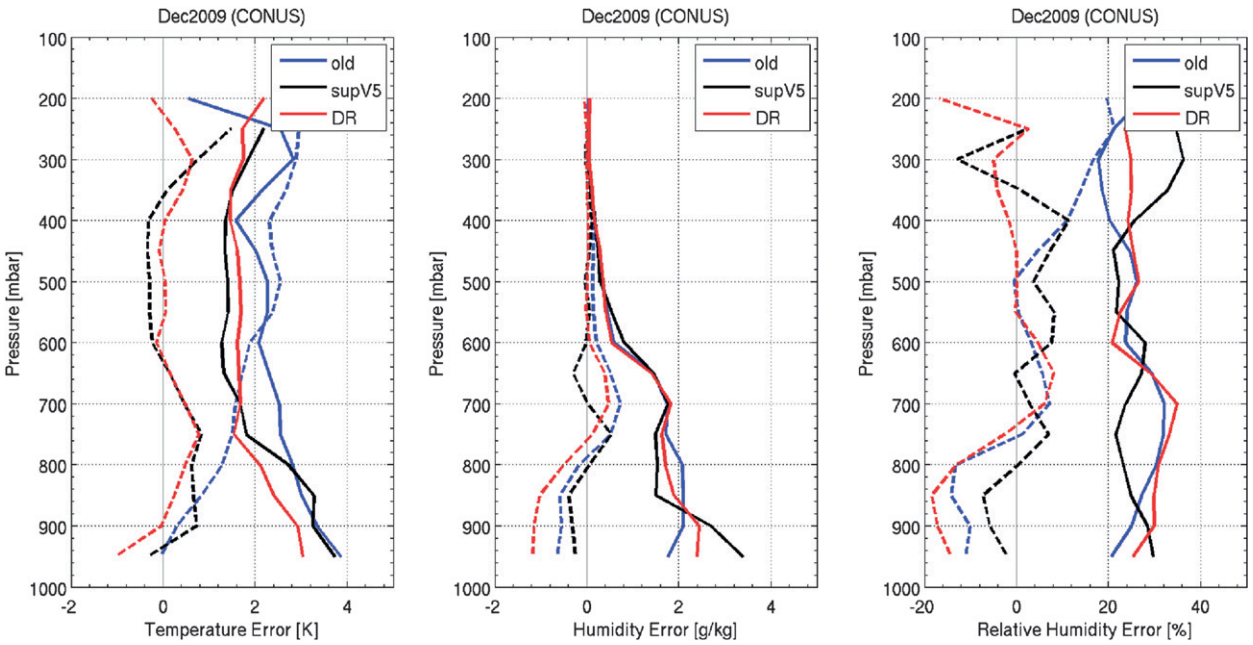

FIG. 7. Comparisons of bias (dashed curves) and std dev (solid curves) of differences between AIRS (left) temperature and (center),(right) water vapor retrievals with radiosonde observations for December 2009 for the CONUS. Three retrieval types are shown: original IMAPP (old) in blue, NASA operational version 5 (supV5) in black, and DR in red.

400–600, 500–700, 600–800, and 700–900 hPa and from 800 hPa to the surface. Thus, a mixture of cloud phases is contained within the 400–600-hPa cloud-height class.

For the clear set of soundings, the surface skin temperature was assigned using a relationship between the surface skin temperature and air temperature derived for the U.S. Department of Energy Oklahoma Atmospheric Radiation Measurement Program Cloud and Radiation Test Bed (ARM/CART) site (Borbas et al. 2005). For the cloudy set of data, the surface skin temperature was assigned using the relationship $T_{\text{skin}} = T_{\text{air}} + \eta(T_{\text{air}})$, where $\eta(T_{\text{air}})$ is a random number with a mean of 0 and a standard deviation std dev $= 0.05(T_{\text{air}} - 200)$ for land and std dev $= 0.015(T_{\text{air}} - 200)$ for water. The surface emissivity was prescribed using a global land surface spectral emissivity database (Seemann et al. 2008) and the standard seawater emissivity spectrum (Wu and Smith 1997). Random variability of the assigned surface emissivity spectrum was produced by multiplying the emissivity spectrum by a random factor $(1 + f)$, where f is a random number taken from a Gaussian random distribution having a mean value of 0 and an std dev of 0.001. The surface reflectivity was assigned from a uniform distribution of random numbers ranging between its specular value of 1 − the emissivity and its diffuse value of (1 − the emissivity)/π.

The CO_2 concentration was treated as a variable ranging between 360 and 400 ppmv. The retrieval regression training datasets (clear and cloudy) have been classified into five different CO_2 categories. The categories are defined by the annual mean values of five 4-yr overlapping periods, the years ranging from 2002 up to 2013. The five overlapping datasets include CO_2 concentration amounts corresponding to years 2002–05, 2004–07, 2006–09, 2008–11, and 2010–13. For each year, the annual mean values have been acquired online (ftp://ftp.cmdl.noaa.gov/ccg/co2/trends/co2_annmean_gl.txt). For the years not included in this list, values have been estimated according to 370 + 2(year − 2000). In the generation of the radiances for each of the five CO_2 classifications, the CO_2 concentration has been randomly assigned using the mean value for each of the four years within each class, with a random perturbation added for which the std dev of the perturbation is 4 ppmv. Thus, for each CO_2 classification, the mean value for each of the four years within the classification, plus its random perturbation, is assigned to all of the atmospheric profiles within the training dataset. In the retrieval step, the set of regression coefficients associated with the radiance observation year (i.e., 1, 2, 3, 4, and 5 for years 2002–04, 2005–06, 2007–08, 2009–10, and 2011–12, respectively) is used.

d. Radiative transfer calculations

Clear-sky-condition radiances are calculated using the Stand-Alone AIRS Radiative Transfer Algorithm (SARTA; Strow et al. 2003). Cloudy-sky radiances are

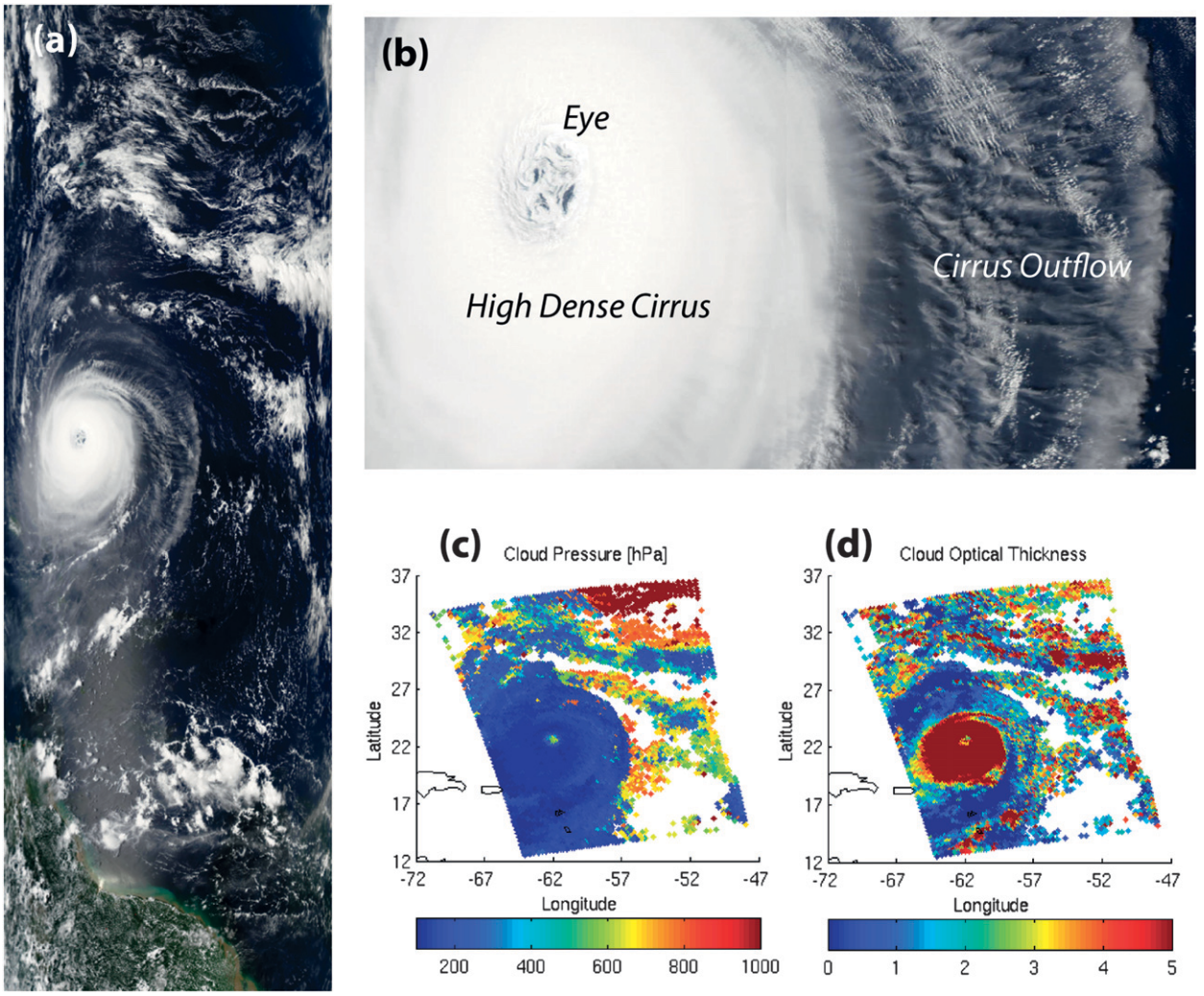

FIG. 8. Satellite imagery of hurricane Isabel (1710 UTC 13 Sep 2003): (a),(b) MODIS 1-km visible imagery (from http://modis.gsfc.nasa.gov/), and AIRS (granules 171 and 172) DR-derived (c) cloud-height pressure and (d) cloud optical depth imagery.

calculated using SARTA for the molecular radiance component combined with a fast cloud radiative transfer model for ultraspectral IR sounder measurements that was developed by Texas A&M and the University of Wisconsin (Wei et al. 2004). For ice clouds, the bulk single-scattering properties of ice crystals are derived by assuming aggregates for large particles (>300 μm), hexagonal geometries for moderate particles (50–300 μm), and droxtals for small particles (0–50 μm) (Yang et al. 2001, 2003). For water clouds, spherical water droplets are assumed, and the classical Lorenz–Mie theory is used to compute their single scattering properties. In the model input, the cloud optical thickness is specified in terms of its visible optical thickness at 0.55 μm. The IR cloud optical thickness for each spectral channel can be derived through the relationship $\tau = \tau_{\text{vis}}(Q_e/2)$, where τ is the cloud optical thickness and Q_e is the bulk mean extinction efficiency. Given the visible cloud optical thickness and the cloud-particle diameter, the IR cloud optical thickness, the single-scattering albedo, and the asymmetry factor can be obtained from a prescribed parameterization of the bulk radiative properties of ice clouds and water clouds. The detailed parameterization scheme has been reported in previous work (Wei et al. 2004). The cloudy radiance for a given spectral channel can be computed by coupling the clear-sky optical thickness and the cloud optical effects. The cloud optical effects are accounted for by using a precomputed lookup table of cloud reflectance and transmittance on the basis of fundamental radiative transfer principles. The clear-sky optical thickness is derived using SARTA, which has 100 pressure layers (101 pressure levels), with vertical coordinates from 0.005 to 1100 hPa. Both the clear-sky and

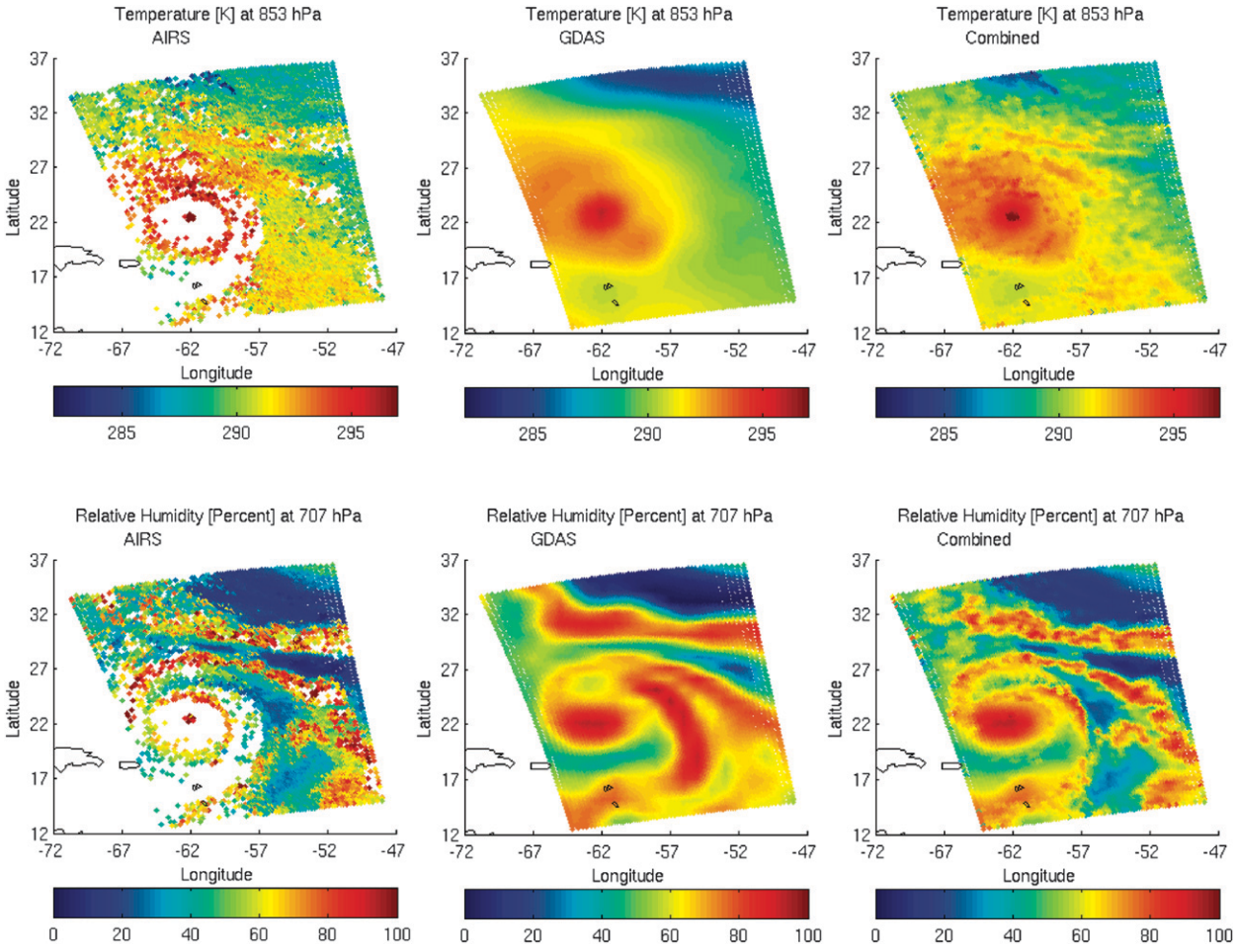

FIG. 9. Comparisons of (left) AIRS (granules 171 and 172; 13 Sep 2003) DR (top) temperature at 853-hPa and (bottom) relative humidity at 707-hPa with the (center) final 1800 UTC operational analyses produced by NCEP's GDAS. (right) The result of combining the AIRS DR retrieval with the NCEP analyses.

cloudy-sky radiance computations take into account the satellite zenith angle, absorption by well-mixed gases (including nitrogen dioxide, methane, silicon dioxide, the chlorofluorocarbons, etc.), water vapor (including the water vapor continuum), ozone, carbon dioxide, and carbon monoxide. Cloudy coefficients are computed for 11 scanning angles within the 0°–50° range, 9 cloud classes, and 5 CO_2 classes. Clear coefficients are obtained for 6 brightness temperature (BT) classes (on the basis of the BT in the window region around 910 cm^{-1}; Weisz et al. 2007a), 11 scanning angles, and 5 CO_2 classes.

e. Final retrieval criteria

The following criteria are applied for producing the "final" combined clear-trained and cloud-trained retrieval:

1) The temperature-profile-defined cloud top is the highest atmospheric level for which the difference between the cloud-trained and the clear-trained retrievals differ by more than 3 K at all levels below that level. The 3-K criterion was based on minimizing the differences between the AIRS-derived cloud-top heights and those observed within the AIRS field of view by the Cloud-Aerosol Lidar with Orthogonal Polarization (CALIOP) instrument (Winker et al. 2003).
2) If the maximum difference between the clear-trained and cloud-trained retrieved surface skin temperature is less than 2.5 K, the clear-trained retrieval is accepted as the final retrieval for all atmospheric levels; otherwise, the clear-trained retrieval is accepted as the final retrieval above the cloud top and the cloud-trained retrieval is accepted as the final retrieval at and below the cloud-top level. Exceptions to this rule occur: (i) if the cloud-top pressure is at or above the 300-hPa altitude, the cloud-trained

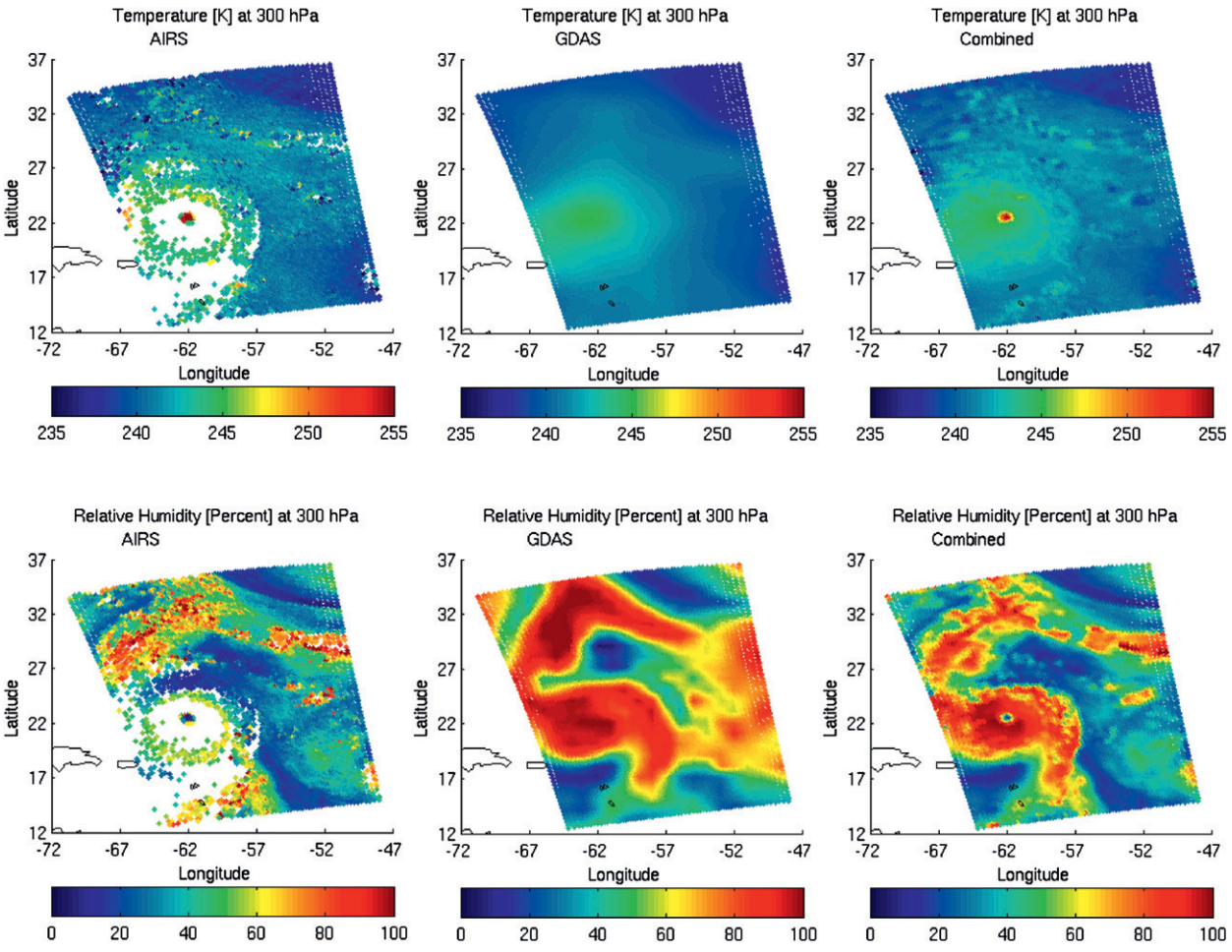

FIG. 10. As in Fig. 9, but for 300 hPa for both variables.

retrieval is accepted as the final retrieval for all atmospheric levels above, at, and below the cloud-top level, and (ii) if the maximum difference between the clear-trained and cloud-trained temperature retrieval exceeds 25 K, the final retrieval below the cloud top is set equal to missing.

3) A relative humidity–defined cloud top is defined as the highest level above the 300-hPa level and above the temperature-profile-defined cloud-top level at which the cloud-trained retrieved relative humidity is equal to, or exceeds, 70%.

f. Quality control

Quality control (QC) is exercised using a number of criteria with the result summarized in a quality-control flag. The quality flag contains three elements. The first element can have a value of 0 or 1 corresponding to good or bad radiances. If this value is 1 then no retrieval is performed, that is, all of the parameters are set to fill values. The second element is associated with partially cloudy conditions. If cloudy retrievals below the cloud top are available then a comparison with the NCEP GDAS profile is performed. The criterion used is based on the vertical mean difference and vertical std dev of the difference between the retrieval and GDAS below the cloud relative to that agreement above the cloud. Value 0 refers to good agreement (i.e., a difference below the cloud that is less than 1.5 times the difference above the cloud), and value 1 refers to not-so-good agreement (i.e., a difference below the cloud that is greater than or equal to 1.5 times the agreement above the cloud) with the NCEP GDAS. A fill value (-9999) is used if no comparison could be performed (i.e., under clear conditions or opaque cloudy conditions). The third element can assume values 0, 1, 2, or 3 on the basis of a cloud-thickness delta ratio (ratio between the "retrieved skin temperature minus GDAS skin temperature" and the "retrieved temperature at cloud top minus GDAS skin temperature"). For ratio ≤ 0.25, $0.25 <$ ratio ≤ 0.5,

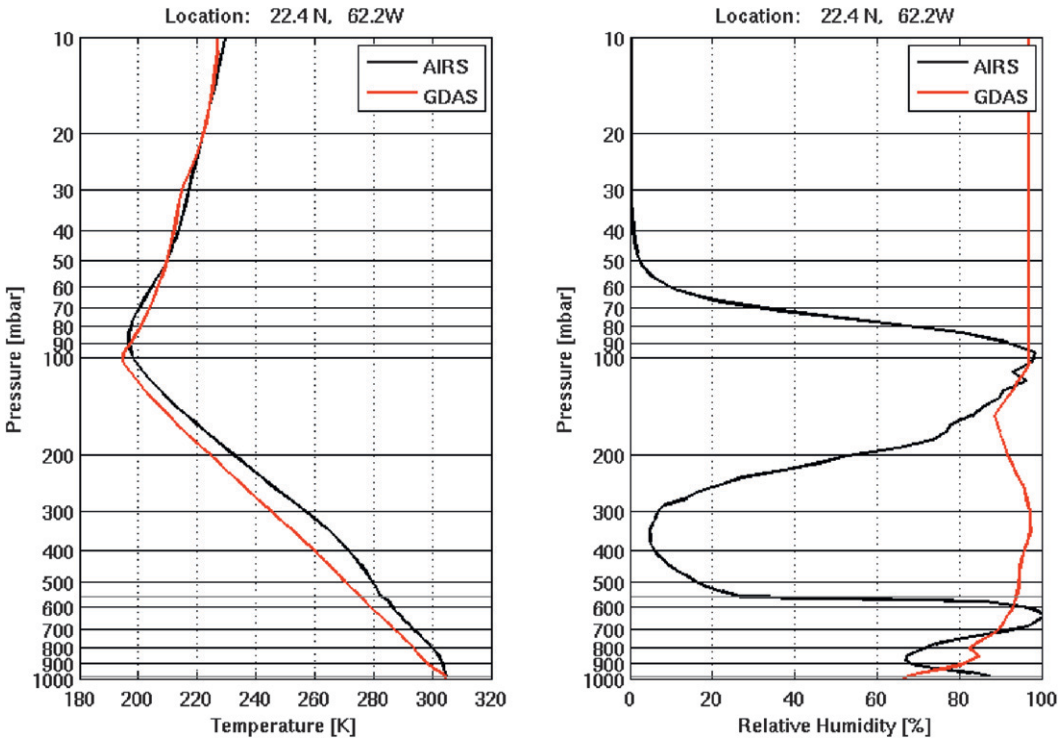

FIG. 11. AIRS sounding retrievals from the eye of Hurricane Isabel (black curves) in comparison with the NCEP GDAS analysis (red curves) for (left) DR temperature and (right) relative humidity.

$0.5 <$ ratio ≤ 0.75, or ratio > 0.75, the quality flags are set to 0, 1, 2, or 3, respectively. Thus a value of 0 refers to clear or thin cloud conditions, whereas a value of 3 refers to thick clouds. It is left up to the user to decide whether to apply any or all of these QC criteria depending on the application of these profiles.

3. Comparison of DR and the original IMAPP retrievals

Retrieval-error statistics were derived for the profile, cloud, and surface conditions forming the training dataset. To achieve these statistics, random radiance errors were added to the radiances calculated from the training dataset, and these radiances were used for the retrieval without any other information regarding cloud or surface condition being provided for the retrieval. The retrievals were performed using both the original unstratified-by-cloud-height regression method (Weisz et al. 2007b) and the stratified-by-cloud-height DR method.

Figure 4 shows the results for the entire training dataset including all clear and cloudy profile conditions, without any QC. Retrievals obtained by the original method were only considered for those levels for which the DR method provided a valid profile result to ensure the comparisons between the original and the DR with the training-dataset ''truth'' profiles are for exactly the same atmospheric conditions. As can be seen, the DR method of retrieval is significantly more accurate than the original unstratified method, particularly for the lower troposphere, where temperature and mixing-ratio error reductions of more than 1° and 0.5 g kg^{-1} are achieved for temperature and water vapor mixing ratio, respectively. One exception to this consistent improvement appears in the bias error for the humidity of the lower troposphere, although the std dev of the retrieval error remain consistently better for the DR-retrieval method. It is important to note that a ''bias correction,'' based on the difference between observed and calculated radiances and often applied by users of the satellite radiance data, is not applied here. Note also that even though Fig. 4a is based on the dependent dataset used to derive the retrieval coefficients virtually the same results are achieved when using an independent sets of data as shown by comparisons of Fig. 4b with Fig. 4c. Here it is shown that virtually identical retrieval-error statistics are obtained for a small portion (25%) of the entire statistical sample retrieved using both statistically independent and dependent sample-based-retrieval coefficients.

Figures 5a–c show, respectively, the temperature, humidity, and relative humidity root-mean-square error (RMSE) statistics classified for the eight different cloud

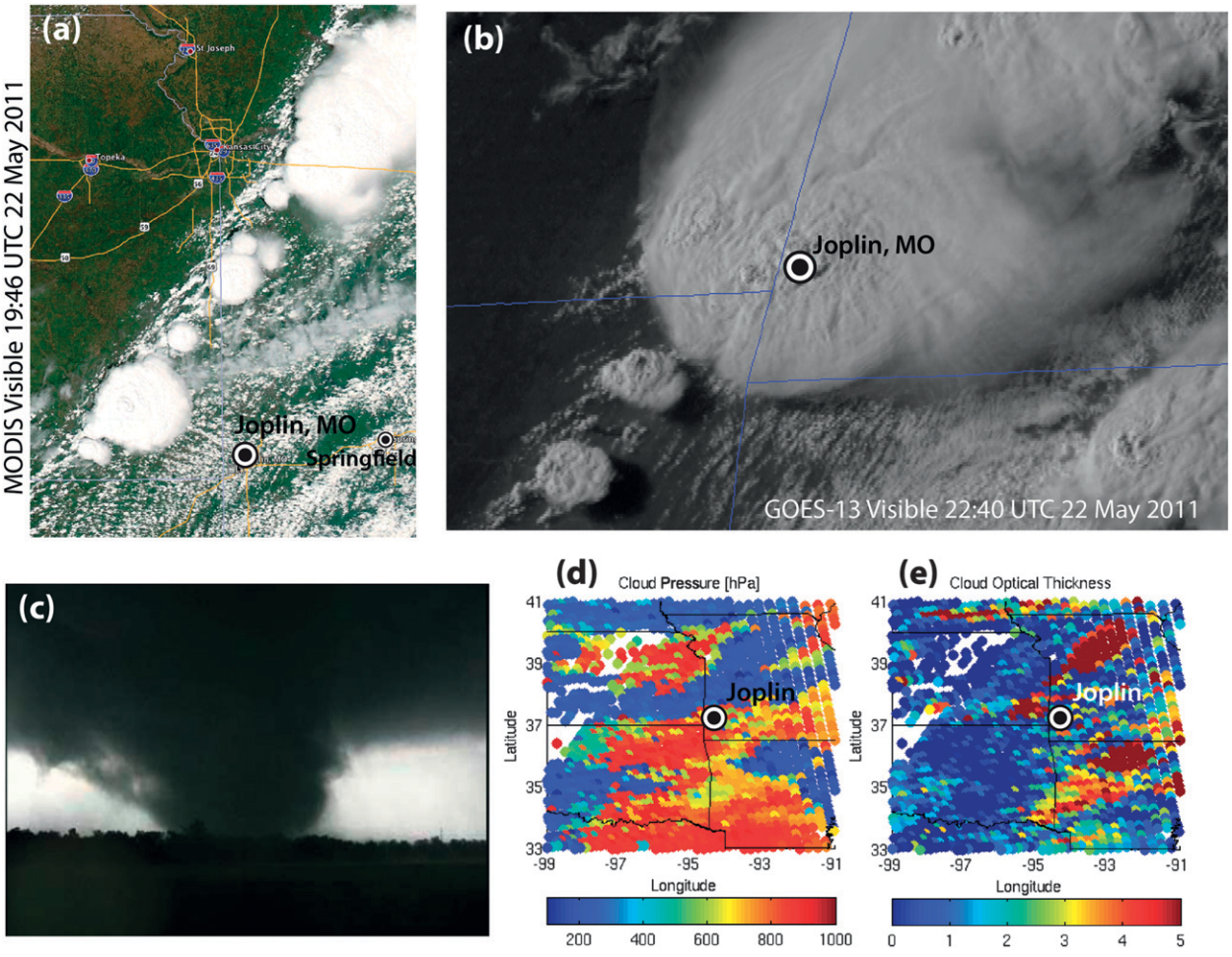

FIG. 12. Satellite imagery (from http://cimss.ssec.wisc.edu/goes/) associated with the Joplin tornado (22 May 2011): (a) MODIS 1-km true-color visible imagery; (b) Geostationary Operational Environmental Satellite visible imagery; (c) an image of the tornado taken by a ground observer, and AIRS (granule 197) DR-derived (d) cloud-height pressure and (e) cloud optical depth imagery.

categories assumed for the DR retrieval. These statistics should be considered as representative of ''worst case'' conditions since no QC has been used to filter out erroneous results. The classification is based on the retrieved, rather than the actual, cloud category so that these error statistics could be used for the expected error of the retrieved profiles as needed for combining them with other sounding data within a data assimilation system. As can be seen, the DR lower-tropospheric temperature profile accuracy is significantly better than the original retrieval accuracy for all cloud conditions, with the improvements being as much as a factor of 2 (i.e., 100%) for most cloud conditions. On the contrary, the DR relative humidity accuracy improvements relative to the original retrievals are confined to the upper troposphere above the cloud levels, indicating that below clouds compensating errors in mixing ratio are associated with the errors in temperature (i.e., values of saturation mixing ratio). That is, below clouds if the original temperature-profile-retrieval error is too high then a too-high mixing-ratio-profile error results, causing the error from the relative humidity profile to be largely unaffected. It is seen that above cloud levels the accuracy of the DR relative humidity retrieval is much better than the original retrieval accuracy, with the improvements being as much a 100% (i.e., 20% in absolute value for DR relative humidity errors near 20%, or less). Although the error statistics for the retrievals that are based on simulated radiances for the training dataset have little day-versus-night or water-versus-land dependence (not shown here), one expects real data-sounding retrievals to be somewhat more accurate in the lower troposphere over water than over land because of the much greater variability of the land surface emissivity relative to ocean emissivity, which must be accounted for in the regression retrieval. Further analysis of real data-retrieval comparisons with

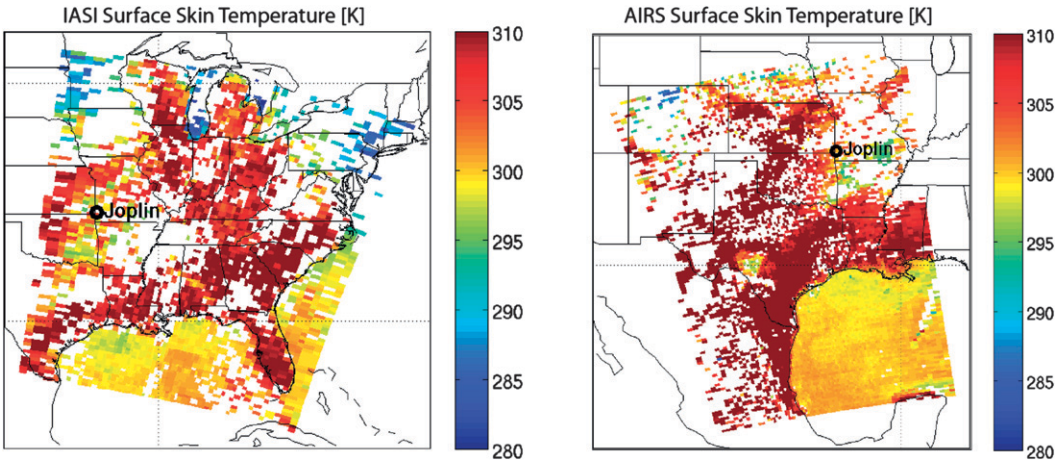

FIG. 13. (left) IASI and (right) AIRS data coverage for the 22 May 2011 Joplin tornado case study. Shown is the derived surface skin temperature, which depicts all of the soundings that were retrieved down to the earth's surface. White areas denote the existence of dense cloud that limited the downward vertical extent of the sounding retrievals to the cloud-top level.

radiosondes (such as shown in Figs. 7 and 17, described below) are needed to define the accuracy dependence on surface type, geographical position, and season.

The DR method relies on being able to diagnose the correct cloud altitude from the radiance spectrum. As described earlier, there are two different cloud estimates obtained with the DR method: the temperature-profile cloud height, which works very well for all but relatively transparent cloud conditions, and the cloud height from the relative humidity profile, which enables the height of relatively transparent clouds to be diagnosed. A common occurrence is the existence of relatively transparent cirrus cloud above a more opaque lower cloud. The combination of the relative humidity cloud height and the temperature-profile cloud retrievals enable this common multilevel cloud-height condition to be retrieved.

Figure 6 shows a comparison of the DR cloud heights and observations from CALIOP on *Cloud–Aerosol Lidar and Infrared Pathfinder Satellite Observations* (*CALIPSO*) and the cloud-profiling radar (CPR) on *CloudSat* for two different AIRS granules. Granule 124 (Fig. 6, top) and granule 187 (Fig. 6, bottom) represent a polar case and a tropical case, respectively. Remember that the field of view of the AIRS (15 km) is much larger than that of the CALIOP (from 333 m to 5 km) and CPR (1.4 km) so that an exact cloud-condition measurement correspondence is not achievable. Also, it is difficult to sense clouds with small optical thickness, as can be detected by the CALIOP, using satellite infrared measurements (Holz et al. 2006). Nevertheless, it is easily seen that the DR temperature-profile cloud heights (red symbols) and the cloud heights from the relative humidity profile (yellow symbols) are in general agreement with the active lidar and radar observations. Most important, it is seen that the DR cloud-height retrievals are in much better agreement with the lidar and radar observations than are the cloud heights derived by the original (old) unstratified-by-cloud-height regression method.

A comparison is also made between the DR regression retrievals for all AIRS granules obtained over the continental United States (CONUS) during December of 2009. The ground truth used was radiosonde observations within ±111 km and ±3 h of the satellite observations. The number of comparisons used to provide these statistics ranged from 100 to 200, depending on atmospheric level. Because the AIRS observations over the CONUS are nominally between 1900 and 2200 UTC, there are large time discrepancies between the AIRS retrievals and the radiosonde observations, leading to the relatively large profile discrepancies shown in Fig. 7, particularly in the surface boundary layer where strong diurnal variations occur. It is still useful to see how the new DR retrieval discrepancies with radiosonde observations compare with those between the original unstratified-regression retrieval method and those associated with the latest available version of the NASA AIRS science-team physical (supV5) retrievals (Susskind et al. 2011). As can be seen, the DR temperature retrievals compare most favorably to the radiosonde observations for temperature, particularly for the lower troposphere. This result holds for both the bias and std dev of the differences. For relative humidity, the results are mixed, probably the result of the compensation discussed earlier that takes

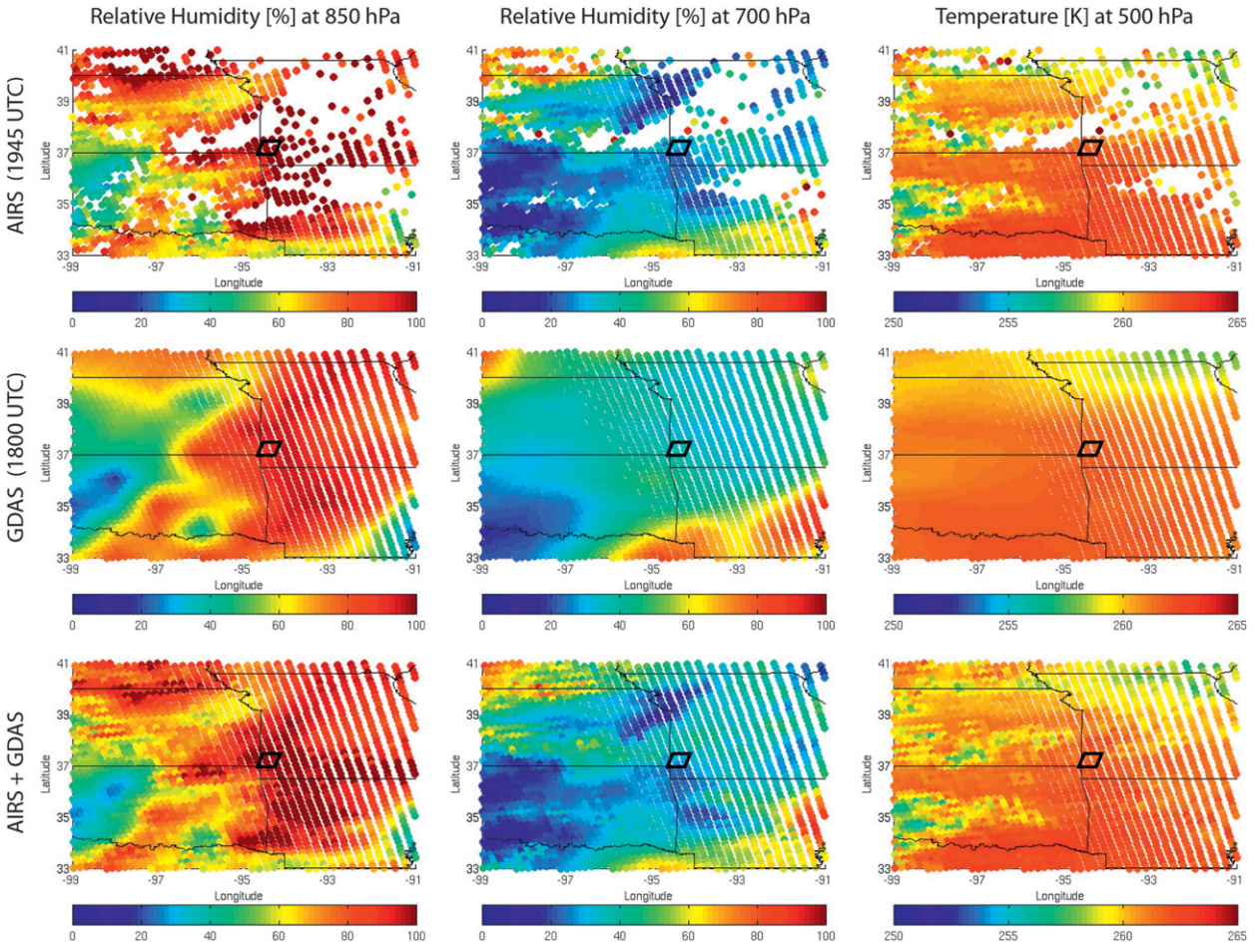

FIG. 14. Example comparisons of (left) relative humidity at 850 hPa, (center) relative humidity at 700 hPa, and (right) temperature at 300 hPa for (top) AIRS DR retrievals, (middle) soundings at the AIRS sounding locations obtained from the final 1800 UTC operational analyses produced by NCEP's GDAS, and (bottom) the combined AIRS DR retrievals and NCEP analysis soundings. White streaks are due to the larger geographical gaps between the AIRS sounding locations that occur near the edge of the scan lines.

place between temperature and mixing-ratio errors within any retrieval method to satisfy the radiance observations.

4. Applications to intense-weather situations

a. Hurricane Isabel

Hurricane Isabel (Fig. 8) was the costliest and deadliest hurricane in the 2003 Atlantic Ocean hurricane season (http://www.nhc.noaa.gov/2003isabel.shtml). Isabel formed near the Cape Verde Islands from a tropical wave on 6 September 2003 in the tropical Atlantic Ocean. It moved northwestward, and within an environment of light wind shear and warm waters it steadily strengthened to a category-5 storm with winds that peaked at 165 mi h^{-1} (265 km h^{-1}) on 11 September. Isabel gradually weakened and made landfall on the Outer Banks of North Carolina with winds of 105 mi h^{-1} (165 km h^{-1}) on 18 September. The worst of the effects of Isabel occurred in Virginia, especially in the Hampton Roads area and along the shores of rivers as far west and north as Richmond and Washington, D.C. Virginia reported the most deaths and damage from the hurricane. Throughout the path of Isabel, damage totaled about $3.6 billion [in 2003 U.S. dollars (USD), equivalent to $4.3 billion in 2011 USD]. Sixteen deaths in seven U.S. states were directly related to the hurricane, with 35 deaths in six states and one Canadian province indirectly related to the hurricane.

The AIRS instrument overflew Hurricane Isabel, and the radiance spectra obtained were used to test the utility of the DR retrieval method for this severe-storm situation. The results presented here are for AIRS granules 171 and 172 at 1710 UTC 13 September 2003. As can be seen from Fig. 8, Isabel had a very well-defined ''eye''

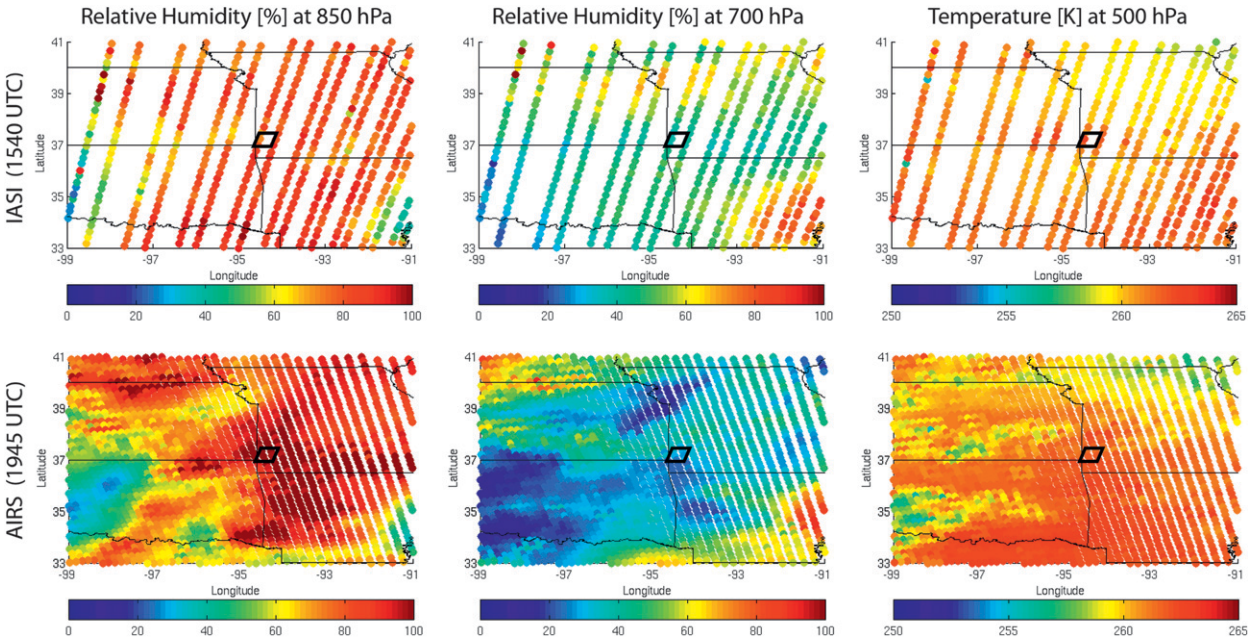

FIG. 15. IASI and AIRS DR derived relative humidity at (left) 850-hPa, (center) relative humidity at 700-hPa, and (right) temperature at 500-hPa obtained using the GDAS 1800 UTC soundings to fill gaps in the satellite sounding data. Shown are (top) the IASI analyses valid at 1540 UTC and (bottom) the AIRS analysis result valid at 1945 UTC, 4 h after the IASI data but 3 h before the tornado. The white areas are due to the geographical gaps between IASI and AIRS sounding locations.

with extremely high cloud cover over the entire region encompassing the storm, including a large cirrus outflow region in which the optical depths of the cloud were relatively small (i.e., <15), thereby permitting many AIRS soundings to be obtained down to near-surface altitudes below the cirrus cloud cover.

Figure 9 shows example AIRS temperature and humidity sounding retrievals (left-hand panels) for low altitudes (i.e., 1.5-km or 853-hPa temperature and 3.0-km or 707-hPa relative humidity). Also shown are the 1800 UTC GDAS analyses (center panels) for the same variables and the combination of the AIRS sounding retrievals and the GDAS analysis (right-hand panels), the GDAS being inserted where there is a void of AIRS soundings. In principle, the AIRS sounding should be assimilated, along with all other available data, into the GDAS but satellite-sounding assimilation is not yet in operational practice. The discontinuities resulting from combining the 15-km-resolution AIRS soundings with the 111-km-resolution GDAS soundings are alleviated by performing a running 3 × 3 (i.e., ~50 km × 50 km) average of the combined profile dataset, producing the result shown in Figs. 9 and 10. As can be seen, the DR retrieval method enables a very large yield in sounding retrievals beneath the cirrus outflow region and within the eye of the storm. This result is significant for improving the definition of the atmospheric thermodynamic structure of the storm. This improvement can be seen by comparing the combined (AIRS + GDAS) data analyses with the GDAS-alone analyses. The combined analyses reveal a much-more-intense hurricane (i.e., warmer eye) with much-more-intense low-level water vapor gradients beneath the cirrus outflow.

Figure 10 shows similar analyses for the 300-hPa level of the atmosphere. It can be seen that for the upper levels of the atmosphere the AIRS data reveal a much-stronger eye, which is barely visible in the GDAS analysis, and much-finer-scale water vapor structure that is not captured in the lower-spatial-resolution (111 km) GDAS analysis. The white areas are regions for which the satellite-sounding vertical extent is limited by clouds to an altitude above that shown. According to Nolan et al. (2009), dropsonde data are available for 13 September to compare with the AIRS retrievals, but this comparison had not been performed by the time of writing of this paper. These comparisons, combined with dropsonde comparisons with AIRS retrievals for a number of other hurricanes within the 2003–11 time period, will be performed and will be the subject of a future publication.

Figure 11 shows a comparison between an AIRS eye sounding and the GDAS analysis at the same location. As can be seen the AIRS temperature within the eye of Isabel is more than 15 K warmer than the GDAS

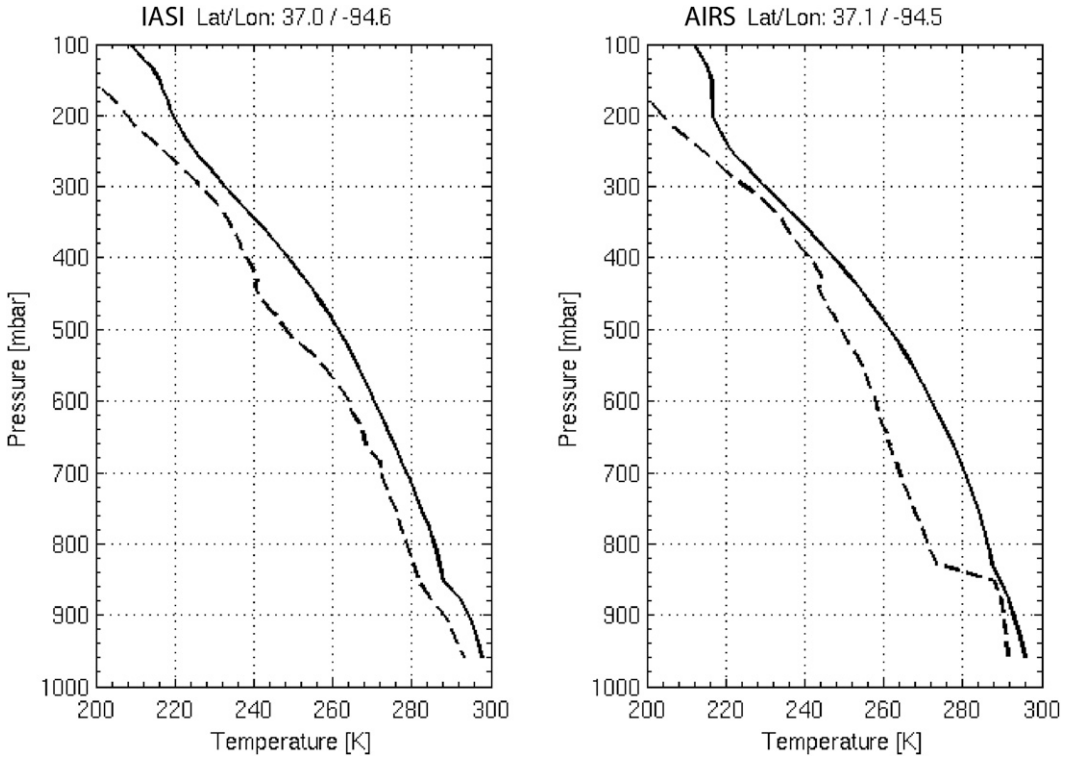

FIG. 16. (left) IASI and (right) AIRS DR-retrieved temperature (solid curves) and dewpoint (dashed curves) profiles at Joplin on 22 May 2011. The IASI sounding was about 8 h prior to the tornado occurrence, and the AIRS sounding was 4 h prior to the tornado occurrence.

analysis, indicating strong subsidence that is associated with an intense storm. Also, the relative humidity retrieved in the eye of the storm is much more realistic, given the known subsidence within the eye, than that provided by the GDAS analyses. The high humidity in the lower troposphere is associated with the low-level cumulus that exists within the eye (see Fig. 8), and the extensive mid–upper-tropospheric dry layer results from the subsidence within the eye of the storm. The relative humidity is also shown to be very high near the tropopause over the eye because of the convergence of moisture from the rainbands surrounding the eye. The GDAS does not reveal these physically expected characteristics of the hurricane because of its relatively poor spatial resolution (~111 km) as well as the lack of sounding data over the ocean influencing the GDAS analyses. Note that AIRS radiance data were not yet being assimilated into the GDAS during the time period of Hurricane Isabel (Le Marshall et al. 2006).

In summary, one can see from the Isabel case study that ultraspectral radiance observations provided by the AIRS can be used to obtain the detailed temperature and moisture structure of the hurricane and its environment, which should lead to improved intensity and track forecasts (Li and Liu 2009).

b. The Joplin tornado

A large portion of Joplin was devastated by an EF-5 (>200 mi h^{-1}; EF denotes the enhanced Fujita damage scale) tornado, resulting in over 160 fatalities and over 900 injured in the Joplin area (http://en.wikipedia.org/wiki/2011_Joplin_tornado) on 22 May 2011. The Joplin tornado (Fig. 12) was the deadliest since modern recordkeeping began in 1950 and is ranked eighth among the deadliest tornadoes in U.S. history. The National Weather Service issued a tornado warning at 1717 central daylight time (CDT) 22 May 2011 for a geographical region that included the city of Joplin. The tornado was reported to have developed directly over Joplin, with the first report of the tornado in Joplin at 1741 CDT 22 May 2011. Although the lead time on the tornado warning was 24 min, this was insufficient time for many people to react to the warning, which may also have been ignored by many because of the fact that the specific location of its formation (i.e., Joplin) could not be forecast coupled with earlier ''false alarms'' (Brotzge et al. 2011).

The question arises as to whether the warning time could be increased through the ''warn on forecast'' approach (Stensrud et al. 2009) by more timely observations of the atmospheric temperature and moisture

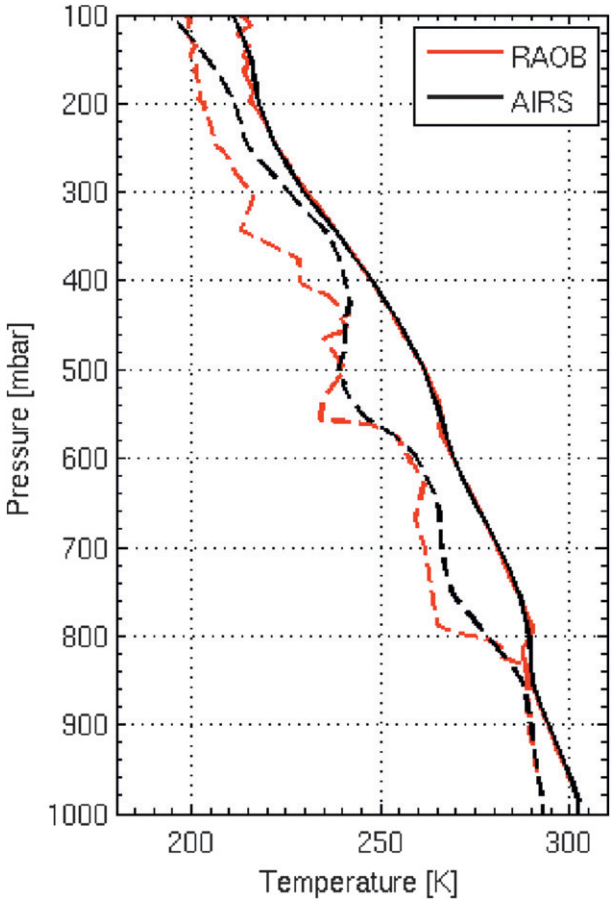

FIG. 17. AIRS DR-retrieved temperature (black solid curves) and dewpoint (black dashed curves) profiles near Springfield at 1940 UTC 22 May 2011 in comparison with a radiosonde observation (red curves) taken at 1800 UTC. Springfield is about 75 mi (~120 km) east of Joplin.

changes associated with tornado formation. On 22 May 2011, the MetOp IASI passed over the Joplin region at 1540 UTC. Four hours later, at 1945 UTC, the *Aqua* AIRS passed over the Joplin region. Although the AIRS observations were still 3 h before the formation of the Joplin tornado, it is of interest to see what changes in atmospheric thermodynamic stability took place between the IASI and AIRS overpass times.

Figures 12d and 12e show the cloud height and effective cloud optical thickness over the Joplin region as retrieved from the AIRS observations (granule 197). One can see from Fig. 12 that there is good correspondence between the cloud-height and optical-thickness retrievals with the MODIS *Aqua* visible imagery. Low scattered-to-broken cumulus clouds existed over Joplin, permitting AIRS single-field-of-view soundings to be obtained down to ground level in near–real time using the DR retrieval method.

Figure 13 shows the surface skin temperature retrieved from IASI (1540 UTC) and AIRS (1945 UTC) data for the MetOp and *Aqua* data granules analyzed for the case study. It serves to illustrate the locations of AIRS and IASI soundings that reached the earth's surface. The coverage of retrieved soundings gets denser at higher altitudes, with complete coverage being obtained above the highest cloud-top altitudes. The geographical consistency between the IASI- and AIRS-retrieved surface skin temperature for common areas (e.g., the western Gulf of Mexico coast, Oklahoma, Louisiana, Arkansas, and Missouri) is particularly noteworthy. A general warming of the earth's land surface is seen, as is expected between the 1540 UTC (1040 CDT) and 1945 UTC (1440 CDT) overpass times while the water temperature remains constant, indicating good absolute calibration consistency between the IASI and AIRS radiance measurements.

Figure 14 shows panels of AIRS-retrieved-sounding values, the GDAS analyses, and GDAS plus AIRS data analyses for the 850-, 700-, and 500-hPa levels. One can see considerable disagreement between the GDAS 1800 UTC 700-hPa relative humidity and 500-hPa temperature analyses and the actual 1945 UTC AIRS sounding data. In particular, the AIRS data show drier and colder (i.e., less stable) upper-level air to the north and west of Joplin than do the GDAS analyses, which did not benefit from these high-vertical-resolution satellite-sounding data.

Figure 15 shows time changes between 1540 and 1945 UTC from the IASI plus GDAS and AIRS plus GDAS analyses. As can be seen, cold/dry air from the west is being advected over a moistening boundary layer at Joplin. This advection of cold, dry air together with the moistening boundary layer over Joplin was instrumental in making the atmosphere over Joplin very unstable with respect to deep convection.

This decrease in the stability of the atmosphere over Joplin is further illustrated in Figs. 16 and 17, which show the changes in the vertical profiles of temperature and dewpoint retrieved over Joplin from the IASI and AIRS radiance measurements. One can see from Fig. 16 that the 1540 UTC IASI sounding provides evidence of a capping inversion at the 850-hPa level, although the entire column of air is relatively moist at the IASI overpass time. At 1940 UTC, the AIRS sounding shows the erosion of the capping inversion and the influence of the strong advection of air above the 850-hPa level, which is much drier than the air observed earlier at the 1540 IASI overpass time. The validity of the DR-sounding retrievals is established by comparison of the AIRS sounding near Springfield, Missouri, about 75 miles east of Joplin, with a special radiosonde observation that was made at 1800 UTC at Springfield. The comparison, shown in Fig. 17, indicates reasonable

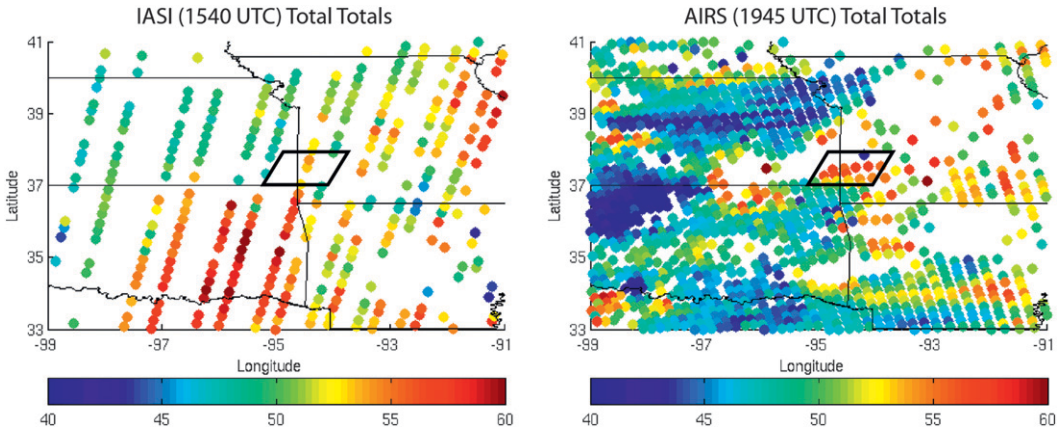

FIG. 18. (left) IASI- and (right) AIRS-derived total totals stability index near Joplin. The white areas are regions in which the satellite-sounding extent is limited by clouds to an altitude above the 850-hPa level used for the total totals calculation.

agreement considering the 2-h time difference between the satellite and radiosonde observations.

Figure 18 shows the time change in atmospheric stability, in terms of the total totals (TT) index, between the IASI 1540 UTC and AIRS 1945 UTC overpass times. The TT index is defined as the difference between the sum of the 850-hPa temperature and dewpoint temperature and 2 times the 500-hPa temperature. Note the large decrease in atmospheric stability (TT increasing from values that are near 50 to values that are near 60), which took place in the vicinity of Joplin between the two satellite overpass times, whereas the stability increased (TT decreasing to less than 50) at most other surrounding locations. There unfortunately were no high-vertical-resolution satellite sounding data between the AIRS 1945 UTC sounding time and the occurrence of the Joplin tornado at 2241 UTC (1741 CDT). Further decreases in atmospheric stability presumably took place, but this decrease cannot be verified because of lack of timely high-vertical-resolution sounding data (Schmit et al. 2009). In any case, the precursor IASI and AIRS sounding-stability diurnal changes prior to the Joplin tornado certainly make a strong case for the need for a geostationary-satellite ultraspectral sounder to better predict the location and timing of severe-weather development. These observations would provide a much earlier warning time than can be issued on the basis of radar and satellite cloud imagery whose observations limit the warning time to that interval after the time the clouds and precipitation associated with the severe weather have already developed.

5. Conclusions

The stratified-by-cloud-height dual-regression retrieval method can be used to produce useful soundings and cloud and surface products in real time from satellite ultraspectral radiance data. The DR capability to retrieve accurate soundings below thin and/or scattered-to-broken cloud is shown to be particularly important for providing the finescale atmospheric-structure information needed to improve hurricane and tornado storm forecasts for these example situations.

It is important to note that the motivation for the DR approach is to enable the real-time production of the desired physical variables (i.e., profiles, and surface and cloud products) from the satellite ultraspectral-resolution radiance measurements. A timing estimate of the DR algorithm indicates that soundings can be produced at a rate of approximately 25 soundings per second on an Apple Mac Pro Quad-Core desktop computer workstation. This rate compares favorably with the 15-sounding-per-second acquisition rate for the AIRS and IASI radiance spectra.

The retrieval algorithm described here is to be integrated into the CIMSS International MODIS/AIRS Processing Package. The DR retrieval algorithm will also form the basis for a new Joint Polar Satellite System Processing Package, which can be used to process MetOp IASI and NPP/JPSS CrIS data.

The results from the application of the method to AIRS and IASI data for two significant intense-weather cases (i.e., Hurricane Isabel and the Joplin tornado) indicate a dramatic improvement in the mesoscale details of the meteorological analyses for both severe-weather situations. Such improvements in analysis detail should have a direct positive influence on forecast accuracy. It is difficult to make such a general conclusion on the basis of only two case-study results, however. The widespread use of satellite-sounding retrievals that are based on the method presented here should enable

a general conclusion to be made regarding the improvement of forecast skill for intense-weather situations using satellite-ultraspectral-sounding data.

Acknowledgments. The development of the DR processing system was made possible through the financial support of NASA and NOAA. The authors are particularly grateful to Drs. Allen Larar, Henry Revercomb, and Allen Huang for their personal interest and encouragement throughout the course of this project.

REFERENCES

Blackwell, W. J., 2005: A neural-network technique for the retrieval of atmospheric temperature and moisture profiles from high spectral resolution sounding data. *IEEE Trans. Geosci. Remote Sens.,* **43,** 2535–2546.

Borbas, E. E., S. W. Seemann, H.-L. Huang, J. Li, and W. P. Menzel, 2005: Global profile training database for satellite regression retrievals with estimates of skin temperature and emissivity. *Proc. 14th Int. ATOVS Study Conf.,* Beijing, China, CIMSS/University of Wisconsin—Madison, 763–770. [Available online at http://cimss.sec.wisc.edu/itwg/itsc/itsc14/proceedings/B32_Borbas.pdf.]

Brotzge, J., S. Erickson, and H. Brooks, 2011: A 5-yr climatology of tornado false alarms. *Wea. Forecasting,* **26,** 534–544.

Chahine, M. T., and Coauthors, 2006: AIRS: Improving weather forecasting and providing new data on greenhouse gases. *Bull. Amer. Meteor. Soc.,* **87,** 911–926.

Hilton, F., and Coauthors, 2012: Hyperspectral earth observation from IASI: Four years of accomplishments. *Bull. Amer. Meteor. Soc.,* **93,** 347–370.

Holz, R. E., S. Ackerman, P. Antonelli, F. Nagle, R. O. Knuteson, M. McGill, D. L. Hlavka, and W. D. Hart, 2006: An improvement to the high-spectral-resolution CO_2-slicing cloud-top altitude retrieval. *J. Atmos. Oceanic Technol.,* **23,** 653–670.

Jin, X., J. Hanesiak, and D. Barber, 2006: Detecting cloud vertical structures from radiosondes and MODIS during CASES field experiment. *Atmos. Res.,* **83,** 64–76.

Le Marshall, J., and Coauthors, 2006: Improving global analysis and forecasting with AIRS. *Bull. Amer. Meteor. Soc.,* **87,** 747–750.

Li, J., and H. Liu, 2009: Improved hurricane track and intensity forecast using single field-of-view advanced IR sounding measurements. *Geophys. Res. Lett.,* **36,** L11813, doi:10.1029/2009GL038285.

Liu, X., D. K. Zhou, A. M. Larar, W. L. Smith, P. Schluessel, S. M. Newman, J. P. Taylor, and W. Wu, 2009: Retrieval of atmospheric profiles and cloud properties from IASI spectra using super-channels. *Atmos. Chem. Phys.,* **9,** 9121–9142.

Minnis, P., Y. Yi, J. Huang, and K. Ayers, 2005: Relationships between radiosonde and RUC-2 meteorological conditions and cloud occurrence determined from ARM data. *J. Geophys. Res.,* **110,** D23204, doi:10.1029/2005JD006005.

Nolan, D. S., J. A. Zhang, and D. P. Stern, 2009: Evaluation of planetary boundary layer parameterizations in tropical cyclones by comparison of in situ observations and high-resolution simulations of Hurricane Isabel (2003). Part I: Initialization, maximum winds, and the outer-core boundary layer. *Mon. Wea. Rev.,* **137,** 3651–3674.

Schmit, T. J., J. Li, S. A. Ackerman, and J. J. Gurka, 2009: High-spectral- and high-temporal-resolution infrared measurements from geostationary orbit. *J. Atmos. Oceanic Technol.,* **26,** 2273–2292.

Seemann, S. W., E. E. Borbas, R. O. Knuteson, G. R. Stephenson, and H.-L. Huang, 2008: Development of a global infrared land surface emissivity database for application to clear sky sounding retrievals from multispectral satellite radiance measurements. *J. Appl. Meteor. Climatol.,* **47,** 108–123.

Smith, W. L., 1991: Atmospheric soundings from satellites—False expectation or the key to improved weather prediction? *Quart. J. Roy. Meteor. Soc.,* **117,** 267–297.

——, and H. M. Woolf, 1976: The use of eigenvectors of statistical covariance matrices for interpreting satellite sounding radiometer observations. *J. Atmos. Sci.,* **33,** 1127–1140.

——, D. K. Zhou, H.-L. Huang, J. Li, X. Liu, and A. M. Larar, 2004: Extraction of profile information from cloud contaminated radiances. *Proc. ECMWF Workshop on Assimilation of High Spectral Resolution Sounders in NWP,* Reading, United Kingdom, ECMWF, 145–154.

——, ——, A. M. Larar, S. A. Mango, H. B. Knuteson, H. E. Revercomb, and W. L. Smith Jr., 2005: The NPOESS Airborne Sounding Testbed Interferometer—Remotely sensed surface and atmospheric conditions during CLAMS. *J. Atmos. Sci.,* **62,** 1118–1134.

——, and Coauthors, 2009: Technical note: Evolution, current capabilities, and future advances in satellite ultra-spectral IR sounding. *Atmos. Chem. Phys.,* **9,** 5563–5574.

Stensrud, D. J., and Coauthors, 2009: Convective-scale warn-on-forecast: A vision for 2020. *Bull. Amer. Meteor. Soc.,* **90,** 1487–1499.

Strow, L. L., S. E. Hannon, S. De Souza-Machado, H. E. Motteler, and D. Tobin, 2003: An overview of the AIRS radiative transfer model. *IEEE Trans. Geosci. Remote Sens.,* **41,** 303–313.

Susskind, J., J. Blaisdell, L. Iredell, and F. Keita, 2011: Improved temperature sounding and quality control methodology using AIRS/AMSU data: The AIRS Science Team version 5 retrieval algorithm. *IEEE Trans. Geosci. Remote Sens.,* **49,** 883–907.

Wei, H., P. Yang, J. Li, B. B. Baum, H.-L. Huang, S. Platnick, Y. Hu, and L. Strow, 2004: Retrieval of semitransparent ice cloud optical thickness from Atmospheric Infrared Sounder (AIRS) measurements. *IEEE Trans. Geosci. Remote Sens.,* **42,** 2254–2267.

Weisz, E., H.-L. Huang, J. Li, E. Borbas, and K. Baggett, 2007a: International MODIS and AIRS processing package: AIRS products and applications. *J. Appl. Remote Sens.,* **1,** 0135519, doi:10.1117/1.2766867.

——, J. Li, J. Li, D. K. Zhou, H.-L. Huang, M. D. Goldberg, and P. Yang, 2007b: Cloudy sounding and cloud-top height retrieval from AIRS alone single field-of-view radiance measurements. *Geophys. Res. Lett.,* **34,** L12802, doi:10.1029/2007GL030219.

Winker, D. M., J. Pelon, and M. P. McCormick, 2003: The *CALIPSO* mission: Spaceborne lidar for observation of aerosols and clouds. *Lidar Remote Sensing for Industry and Environment Monitoring III,* U. N. Singh, T. Itabe, and Z. Liu, Eds.,

International Society for Optical Engineering (SPIE Proceedings, Vol. 4893), 1–11.

Wu, X., and W. L. Smith, 1997: Emissivity of a rough sea surface for 8–13 μm: Modeling and verification. *Appl. Opt.,* **36,** 2609–2619.

Yang, P., B. C. Gao, B. A. Baum, Y. X. Hu, W. J. Wiscombe, S. C. Tsay, D. M. Winker, and S. L. Nasiri, 2001: Radiative properties of cirrus clouds in the infrared (8–13 μm) spectral region. *J. Quant. Spectrosc. Radiat. Transfer,* **70,** 473–504.

——, B. A. Baum, A. J. Heymsfield, Y. X. Hu, H.-L. Huang, S. C. Tsay, and S. Ackerman, 2003: Single-scattering properties of droxtals. *J. Quant. Spectrosc. Radiat. Transfer,* **79–80,** 1159–1169.

Zhou, D. K., W. L. Smith, X. Liu, A. M. Larar, H.-L. A. Huang, J. Li, M. J. McGill, and S. A. Mango, 2005: Thermodynamic and cloud parameters retrieval using infrared spectral data. *Geophys. Res. Lett.,* **32,** L15805, doi:10.1029/2005GL023211.